



The emerging landscape of spatial profiling technologies

Jeffrey R. Moffitt^{1,2}, Emma Lundberg^{3,4,5,6} and Holger Heyn^{7,8}

Abstract | Improved scale, multiplexing and resolution are establishing spatial nucleic acid and protein profiling methods as a major pillar for cellular atlas building of complex samples, from tissues to full organisms. Emerging methods yield omics measurements at resolutions covering the nano- to microscale, enabling the charting of cellular heterogeneity, complex tissue architectures and dynamic changes during development and disease. We present an overview of the developing landscape of *in situ* spatial genome, transcriptome and proteome technologies, exemplify their impact on cell biology and translational research, and discuss current challenges for their community-wide adoption. Among many transformative applications, we envision that spatial methods will map entire organs and enable next-generation pathology.

The architecture of a vast array of different molecules within cells and cells within tissues is an essential determinant of cellular and tissue function. Bulk and single-cell genomic technologies offer the ability to characterize the remarkable diversity of molecules that define cellular identity and function at their native complexity level, the genome scale, which, in turn, has empowered a diverse and exciting range of discoveries. Until recently, these transformative single-cell technologies largely characterized dissociated cells removed from the sample of interest and, as such, came with a natural loss of the spatial context of molecules within cells and of cells within samples — a context that is essential to many biological questions. Spatially resolved genomic methods offer the solution to this challenge, providing genome-scale omics measurements while preserving spatial context (FIG. 1). Excitingly, the discoveries made with these new and rapidly developing methods are likely to complement, and may perhaps even outstrip, the tremendous advances driven by dissociated single-cell methods.

There has been a recent explosion in the diversity and capabilities of spatial omics methods, including various techniques that can now quantify the transcriptome or the proteome and map genome organization across a wide range of scales in a diverse set of tissues. Major limitations such as scale, resolution, sensitivity, multiplexing and diverse-sample applicability are starting to be resolved as these methods mature beyond early proof of principle. Indeed, the latest spatial methods now provide transcriptome- or proteome-wide information across a range of biologically relevant length scales. Moreover, commercial options are increasingly available and, therefore, we anticipate widespread adoption of these technologies over the next few years. With the

goal to perform bias-free, data-driven exploratory cellular phenotyping *in situ*, spatial technologies promise to further transform our knowledge about the complexity of life by holding a magnifying glass to the molecular and spatial architecture of tissues and cells.

In this Review, we provide an overview of the current landscape of spatially resolved genomic, transcriptomic and proteomic methods and cover their important technical and performance features. As the range of demonstrated applications is too diverse to cover in a single review, we highlight illustrative applications to showcase the types of insight such methods promise. To conclude, we discuss the need for coordinated efforts to establish standardized experimental and analysis frameworks and provide a brief perspective of future technological breakthroughs and impact areas. The multidimensional nature and the massive amounts of data produced by these methods dictate that computational efforts go hand-in-hand with experimental methods, although these computational challenges and the exciting range of solutions are beyond the scope of this Review.

Spatial indexing transcriptomics

Advances in the ability to index RNA molecules *in situ* or capture them locally now allows the spatial transcriptome-wide profiling of gene expression in tissues and organs. Mapping indexed sequencing reads back into two dimensions enables the interrogation of regional gene expression heterogeneity and, when combined with single-cell transcriptomics, the disentanglement of cell type colocalization patterns and regionalization. Common to spatial indexing transcriptomics is the barcoding of RNA molecules *in situ* and the subsequent quantification of gene expression profiles using next-generation sequencing (NGS), followed by

¹Program in Cellular and Molecular Medicine, Boston Children's Hospital, Boston, MA, USA.

²Department of Microbiology, Harvard Medical School, Boston, MA, USA.

³Science for Life Laboratory, School of Engineering Sciences in Chemistry, Biotechnology and Health, KTH - Royal Institute of Technology, Stockholm, Sweden.

⁴Department of Bioengineering, Stanford University, Stanford, CA, USA.

⁵Department of Pathology, Stanford University, Stanford, CA, USA.

⁶Chan Zuckerberg Biohub, San Francisco, San Francisco, CA, USA.

⁷CNAG-CRG, Centre for Genomic Regulation (CRG), Barcelona Institute of Science and Technology (BIST), Barcelona, Spain.

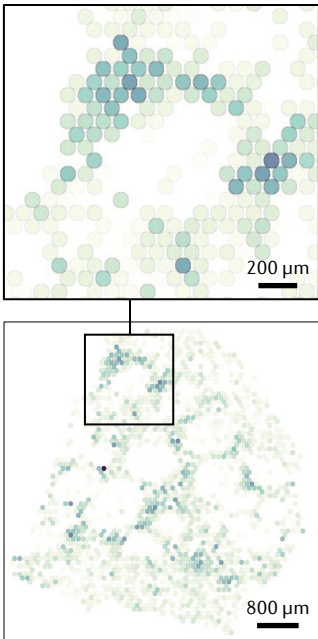
⁸Universitat Pompeu Fabra (UPF), Barcelona, Spain.

✉ e-mail: holger.heyn@cnag.crg.eu

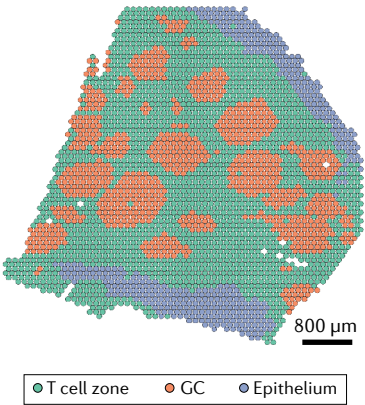
<https://doi.org/10.1038/s41576-022-00515-3>

Spatial indexing methods for tissue atlasing

a Spot-based gene signature mapping through transcriptome capture



b Regional clustering of transcriptomes



c Spot deconvolution for cell type composition inference

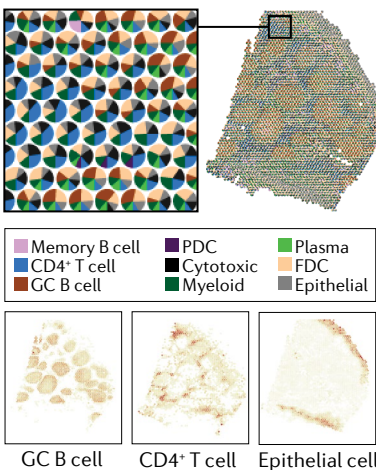
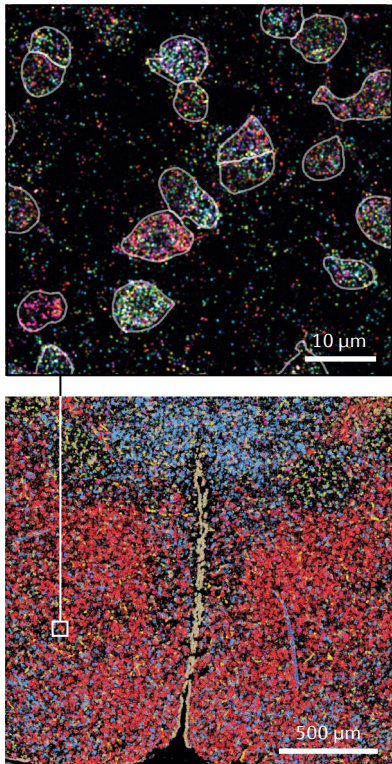


Image-based transcriptome profiling for subcellular and tissue-scale atlasing

d Single-RNA-molecule, subcellular mapping across cm² tissues



e Cell type and state discovery



f Construction of large-scale cellular atlases

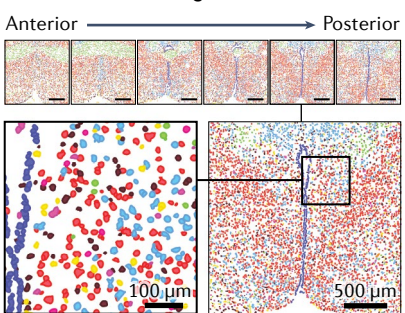
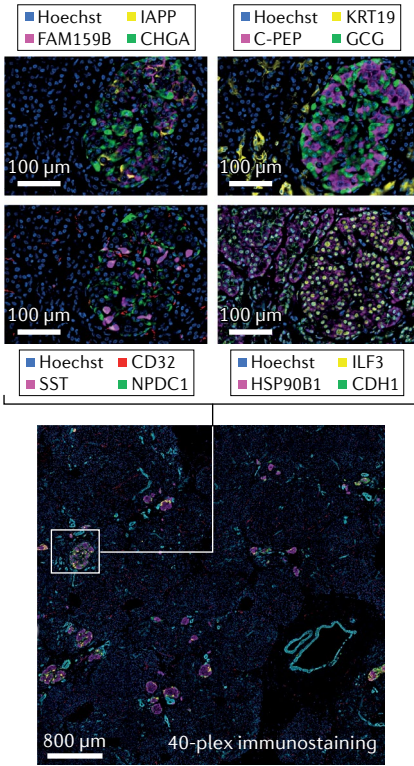
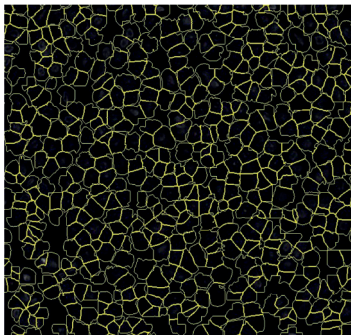


Image-based proteome profiling for subcellular and tissue-scale atlasing

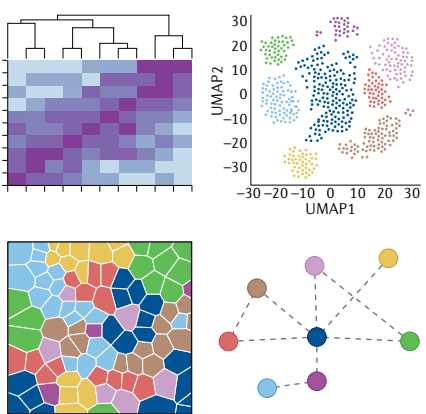
g Multiplex protein detection, subcellular resolution across cm² tissues



h Cell segmentation and type or state classification



i Spatial cell neighbourhood analysis



◀ Fig. 1 | Illustrative examples of spatial profiling measurements. **a** | Single-spot resolution (55 µm spot size, 100 µm centre-to-centre distance) of the Visium spatial transcriptomics platform quantifying the gene expression signature of the T cell zone in a human tonsil. **b** | High-level clustering of spot-based transcriptomes to define functional compartments organized in structural features. **c** | Predicted cell type composition of spots through single-cell reference-based deconvolution²³. **d** | Spatial distribution of 155 RNAs profiled with an image-based transcriptomics method, multiplexed error-robust fluorescence *in situ* hybridization (MERFISH), in the mouse hypothalamus, illustrating the simultaneous subcellular (left) and tissue-scale (right) resolution typical of such techniques¹⁰⁹. **e** | t-distributed stochastic neighbour embedding (tSNE) representation of the cellular expression profiles for measurements taken from the same study as part **d**. Eight cell classes, representing 83 defined cell types, are coloured, illustrating the ability of such methods to define cell types and states with targeted gene measurements¹⁰⁹. **f** | A representative tissue atlas showing the identity (colour) and location of eight cell classes identified in this region of the mouse brain with MERFISH¹⁰⁹. **g** | Spatial proteomics experiment using a 40-plex CODEX assay to visualize cell types and states in human pancreas. **h** | Nuclear and membrane markers are used to derive highly precise cell segmentation masks for single-cell analysis and cell type classification. **i** | Example of typical spatial neighbourhood analysis performed on spatial proteomics data to identify cell types, local cell neighbourhoods and higher order organization of these neighbourhoods. FDC, follicular dendritic cell; GC, germinal centre; OD, oligodendrocyte; PDC, plasmacytoid dendritic cell. Parts **e** and **f** from Moffitt, J. R. et al. Molecular, spatial, and functional single-cell profiling of the hypothalamic preoptic region. *Science* **362**, eaau5324 (2018)¹⁰⁹; modified with permission from AAAS.

Multiplexing

The simultaneous profiling of multiple gene transcripts or proteins through the application of pools with panels of detection probes or antibodies, respectively.

Deterministic barcoding

Flexible profiling of spatial coordinates through the targeted labelling of cells or regions of interest using molecular probes, cell tags or fluorescent markers.

Detection efficiency

In the context of image-based transcriptomics, this concept refers to the fraction of targeted molecules that are present in the sample that are actually detected. As single-molecule fluorescence *in situ* hybridization (smFISH) is often used as a proxy for ground-truth expression, this quantity is often calculated by comparison with smFISH, though comparison with single-cell RNA sequencing is also common. As there is no standard definition in the field, care should be taken in comparing values.

Formalin-fixed paraffin-embedded (FFPE)

Preservation method for tissues in long-term archival storage. After a tissue is collected, it is preserved through formalin fixation to preserve its spatial architecture and finally embedded in a paraffin wax block.

coordinate-specific demultiplexing (that is, assigning sequencing reads to locations based on their spatial index). Here, we zoom in from early protocols with low spatial resolution to recent high-resolution methods that provide single-cell and even subcellular resolution. Furthermore, we distinguish between solid-phase and deterministic barcoding methods as well as elaborate solutions that combine single-cell and spatial transcriptomics (ST) through *in situ* barcoding and dissociation (FIG. 2). Main application areas include charting complex tissue architectures in healthy human organs¹, such as the adult and developmental intestinal tract^{2,3} or the heart in health^{4,5} and after myocardial infarction^{6,7}. Additionally, the study of human tumours and cancer mouse models has contributed to the understanding of tumour cell^{8,9} and microenvironment heterogeneity^{10–13}.

Solid-phase transcriptome capture technologies. ST^{14,15} was the first method to introduce positional molecular barcodes during complementary DNA (cDNA) synthesis and subsequent RNA sequencing readout. Hence, the name is often used when referring to spatial indexing methods in general and, potentially confusingly, to the entire field of spatial RNA profiling. Here, we use ST to refer to the technique for clarity. ST uses immobilized spatially barcoded oligo(dT) primers on a glass surface covered by tissue sections. The first version of ST arrays harboured 1,007 uniquely barcoded spots with a diameter of 100 µm, covering an area of 6 × 6 mm (centre-to-centre distance of 200 µm). Gene detection efficiency compared with gold-standard single-molecule fluorescence *in situ* hybridization (smFISH) revealed 6.9% sensitivity in brain sections, which is comparable to initial versions of single-cell RNA sequencing (scRNA-seq) technologies¹⁴. Furthermore, lateral molecule diffusion of RNA molecules after permeabilization that could produce intermixed gene expression profiles was benchmarked to laser-capture microdissection, confirming reliable spatial transcriptome profiling capacities. For the first time, ST allowed dimensionality reduction of

regional expression profiles and the spatial clustering to infer heterogeneity in transcriptomes (FIG. 1b). As an outlook towards its applicability in digital pathology, ST was applied in breast cancer sections, detecting putative local restriction of cancer subclones.

As a side note, RNA integrity is key for the performance of fresh-frozen ST protocols, traditionally assessed through ribosomal RNA (rRNA) and quantified as RNA integrity number (RIN) from RNA isolated from bulk samples. To conserve the spatial information and to determine spatial differences in sample quality that might introduce regional biases, a modified ST array capturing 18S rRNA has been developed, defining spatial RNA integrity number (sRIN)¹⁶. Furthermore, conserving full-length transcript information, an ST variation termed spatial isoform transcriptomics (SiT) performs both short-read and long-read sequencing to simultaneously profile gene expression and isoform usage pattern in tissue sections¹⁷. Following cDNA amplification, the ST sample is split and subjected to full-transcript and fragmented 3' library preparation. Leveraging the full-length transcriptome information, SiT also enables the interrogation of adenosine-to-inosine RNA editing sites. ST has been commercialized as the Visium platform (10× Genomics) with approximately 5,000 spots of 55 µm diameter (110 µm pitch), increasing resolution and its accessibility. A recurrent limitation of single-cell and spatial technologies is their limitation to fresh-frozen tissue sections, largely excluding formalin-fixed paraffin-embedded (FFPE) samples of clinical cohorts with strong legacy data. To solve this issue for the aforementioned widely used ST method, a modified Visium protocol that captures whole-transcriptome gene-specific probes *in situ* provides a promising solution¹⁸. Alternatively, a modified ST version applies de-crosslinking at high temperatures and specific buffer conditions, which is essential to improve molecule capture from highly crosslinked FFPE samples, before capturing mRNA molecules using standard oligo(dT) capture oligonucleotides¹⁹.

To improve resolution of ST and Visium, Slide-seq²⁰ uses transcriptome capture arrays created from uniquely DNA-barcode 10 µm beads (similar to Drop-seq²¹) loaded onto a rubber-coated glass coverslip. The random spatial barcodes are read through SOLiD (sequencing by oligonucleotide ligation and detection) chemistry before application of snap-frozen sections to the dried bead surface. The method was updated to Slide-seqV2 (REF.²²), with improved indexing and more efficient library preparation to increase molecule capture efficiency. Specifically, bead indexing was modified to make it independent of the proprietary cleavage chemistry of the SOLiD approach and more error-robust. Transcript resolution was enhanced through improved clonality of barcodes and the addition of another second-strand synthesis to increase library complexity.

The above techniques use capture areas with sizes equivalent to a few to many multiple cells. Consequently, the presence of cell types in specific areas has to be inferred. This is achieved through spot deconvolution²³ or gene expression signatures¹⁰ usually defined by single-cell reference data sets (FIG. 1a,c). For example, to integrate Slide-seq with scRNA-seq data sets,

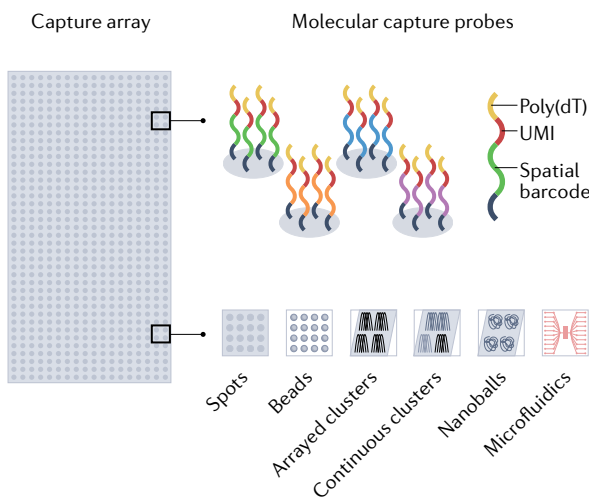
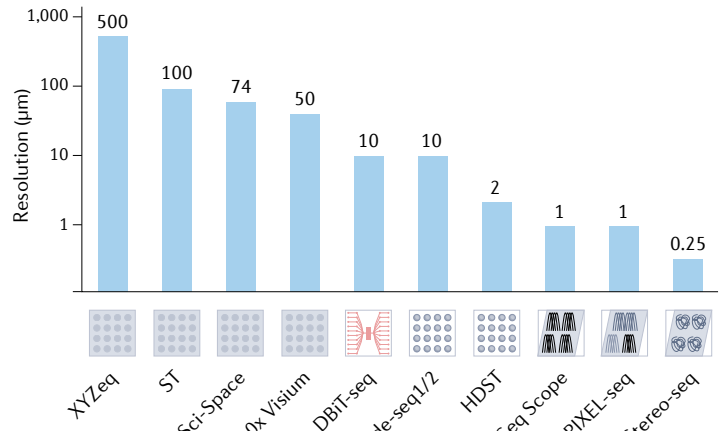
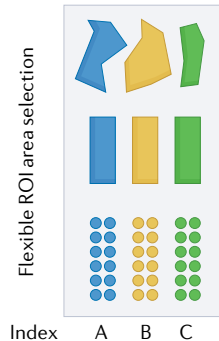
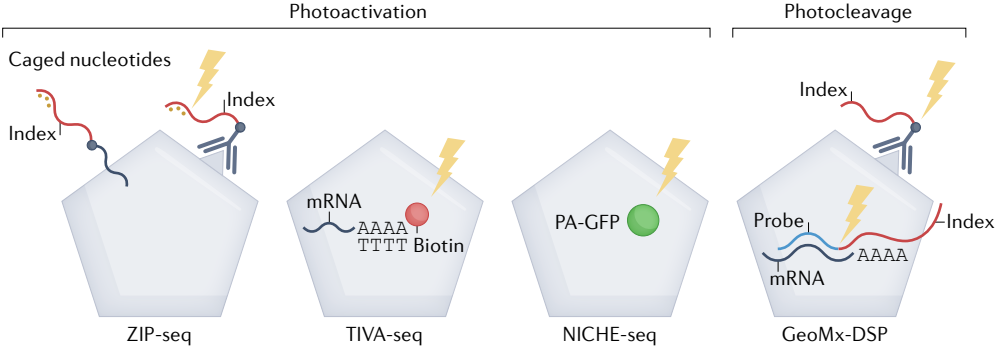
a | Spatial indexing transcriptomics**b | Molecule capture resolution****c | ROI****d | ROI labelling strategies**

Fig. 2 | Spatial indexing strategies. **a |** Spatial indexing arrays capture probe design (top) and array formats (bottom). **b |** From multicell to subcellular transcriptome capture methods. The size of capture areas defines the resolution of cellular transcriptome profiles (y-axis). Larger areas (>10 μm spots or beads) capture a mixture of multiple cells, whereas recent methods provide even subcellular transcriptome profiles (<2 μm clusters). Multicell capture methods can provide single-cell resolution through spatial barcoding with subsequent tissue digestion (XYZeq, sci-Space). Barcoding formats differ between solid-phase capture and deterministic methods (deterministic barcoding in tissue for spatial omics sequencing; DBiT-seq). **c |** Region of interest (ROI) selection and multiplexing. Targeted

selection of regions using photoactivation or photocleavage for flexible area designs. Regional indexing with different barcodes enables multiplexing and pooled downstream processing. **d |** ROI labelling strategies tag molecules (mRNA) or cells (intracellular fluorescent markers or membranes) using photoactivation or photocleavage for subsequent multiplexed next-generation sequencing readout of molecule or cell pools. DSP, digital spatial profiler; HDST, high-definition spatial transcriptomics; PA-GFP, photoactivatable green fluorescent protein; PIXEL-seq, Polony (or DNA cluster)-indexed library sequencing; ST, spatial transcriptomics; Stereo-seq, spatiotemporal enhanced resolution omics sequencing; UMI, unique molecular identifier.

DNA nanoballs (DNBs). Dense clusters of DNA amplified by rolling circle replication used for DNA sequencing or spatial RNA capture.

Rolling circle amplification (RCA). A process by which a circularized single-stranded DNA, such as a padlock probe, is replicated into a long molecule composed of concatenated copies of the circularized probe by extending a bound primer with a polymerase capable of strand displacement.

non-negative matrix factorization regression (NMFreg) was applied with a weighted combination of gene expression signatures of reference single-cell data sets to infer the spatial distributions of neuronal and non-neuronal cell types in a coronal mouse cerebellar section²⁰.

Providing even subcellular resolution and, thus, theoretically enabling direct *in situ* cellular phenotyping, high-definition ST²⁴ uses 2,893,865 individual barcoded beads, generated by split-and-pool reactions, that are randomly placed into hexagonal arrays with >1.4 million 2 μm well bead arrays. Subsequently, the positional barcodes are identified by sequential hybridization rounds, imaging and error correction. Integration with corresponding haematoxylin and eosin (H&E) staining allowed subcellular compartmentalization

and the extraction of nuclear expression features. To achieve even higher spatial resolution below the micrometre scale, spatiotemporal enhanced resolution omics sequencing (Stereo-seq)²⁵ performs *in situ* RNA capture on DNA nanoballs (DNBs) to provide nano-scale resolution in patterned flow cells, similar to those developed for synthesis-by-sequencing solution for NGS²⁶. DNB-loaded arrays contain billions of barcodes with area profiling extendable to the centimetre scale (50–200 mm²), allowing the profiling of small model organisms, whole embryos or organs, as well as the simultaneous capture of multiple smaller samples on the same chip, thereby reducing batch effects^{25,27–29}. Random barcode sequences, generated by rolling circle amplification (RCA), are loaded onto a silicon surface etched with a

grid-patterned array and an approximately 220 nm spot size (centre-to-centre distance of 500–715 nm), generating subcellular transcript profiles. Arrays are imaged and sequenced to obtain the barcode coordinate identity (CID) before ligating molecular identifiers and oligo(dT) oligonucleotides. Current strategies for cell segmentation during data analysis combine nuclei staining and nucleus prediction based on an increased ratio of exonic and intronic reads. In contrast to micrometre-scale technologies, nanoscale techniques require the convolution of subcellular areas to reduce sparsity, to define cell boundaries and for bona fide spatial cell atlas building.

Acting at a similar scale to Stereo-seq, below the micrometre-scale mark, Sequence-Scope (Seq-Scope)³⁰ applies solid-phase amplification of randomly barcoded single-molecule oligonucleotides using the MiSeq Illumina sequencing-by-synthesis platform³¹ to generate pixels approximately 0.5–1 μm apart from each other and up to 1.5 million different spatially defined barcodes in a 1 mm² area (150 pixels in a 100 μm² area). Specifically, seed oligonucleotide libraries with random spatial barcodes are amplified on a PCR adapter-coated solid surface to produce clusters for subsequent digestion and molecule capture from frozen sections. Random primer sequences are used for second-strand synthesis and also serve as unique molecular identifiers. Subcellular localization could be partially resolved through ratios of exonic to intronic reads (nucleus versus cytoplasm) and known organelle-specific transcripts (mitochondria). Subcellular resolution is also achieved using Polony (or DNA cluster)-indexed library sequencing (PIXEL-seq)³², which uses NGS technology to produce ultra-dense arrays with polymerase-amplified oligonucleotide colonies (known as polonies³³) of <1 μm diameter. Unlike traditional sequencing arrays with discrete and non-homogeneous DNA distributions, PIXEL-seq generates continuous homogeneous polonies across a customized gel surface. Continuous polonies are connected but rarely interpenetrate and can be efficiently cleaved by restriction digestion to create oligo gels for RNA capture. PIXEL-seq randomly seeds clusters on a gel of customizable size (for example, 6 × 30 mm²) arrays with a feature density of ~0.5 million mm⁻² and average size of 1.17 ± 0.1 μm². Of note, nanoscale methods differ in cluster density, but also in the number of spatially barcoded capture oligos per cluster, with Illumina technology (Seq-Scope) generating in the range of thousands and PIXEL-seq generating >20,000 oligos per cluster. Although nanoscale data are extremely sparse per capture unit, accumulating transcript counts across cell segments or micrometre-scale tiles results in transcriptome profiles comparable to those of other spatial indexing techniques. However, systematic benchmarking across methods would be required to draw general conclusions about the respective capture performance of different methods.

Although the above-mentioned methods generate spatial profiles at even subcellular scale, they do not provide bona fide single-cell transcriptomes, as cell segmentation algorithms need to infer cell boundaries. This limitation has been addressed by combining spatial molecule indexing with subsequent tissue digestion

and scRNA-seq. XYZeq encodes spatial information into scRNA-seq libraries using two rounds of split-pool indexing³⁴. First, after reversible crosslinking of 25 μm tissue slices, the spatial location is incorporated by *in situ* reverse transcription in uniquely barcoded microwells (500 μm centre-to-centre distance). Then, tissues are digested and cell pools are distributed into wells and subjected to a second indexing round by PCR to generate unique combinatorial barcodes. Specifically, 768 spatial indexes and 384 PCR indexes generate up to 294,912 unique single-cell barcodes. Mixed-species experiments pointed to certain cross-contamination between cells, which could be reduced using computational correction (DecontX). As an alternative with even greater scalability of cell numbers, sci-Space³⁵ uses spatially arrayed indexed oligonucleotides that are diffused into the nuclei of juxtaposed sections to barcode their spatial position. Oligos are spotted onto glass slides coated with dried agarose, resulting in a grid of spots with a mean radius of 73 μm. Following diffusion transfer of the spatial indexes, the nuclei are extracted, fixed and used for single-nucleus RNA-seq through combinatorial indexing with sci-RNA-seq protocol. Compared with the above-utilized commercial droplet-based scRNA-seq³⁶, the established workflow can be scaled more cost efficiently, allowing larger area and cell numbers to be profiled. Of note, although both digestion-based methods generate single-cell-resolved profiles, their spatial resolution is restricted to the size of the indexing area (500 μm and 73 μm, respectively) and, therefore, they do not provide bona fide spatial single-cell profiles.

Deterministic spatial barcoding technologies. Whereas the above solid-phase methods capture RNA molecules with a predefined grid of spatially indexed probes, deterministic methods are flexible in their capacity to deliver barcodes to cells or regions of interest (ROIs). Capturing cells with reasonably dense spatial information has been traditionally achieved using laser-capture microdissection³⁷ and patch-pipette aspiration^{38–40}. Scaling this to single-cell-resolved spatial transcriptomes, TIVA-seq⁴¹ isolates mRNA from a single cell using photoactivatable mRNA capture molecules. Specifically, an uncaged oligonucleotide anneals to the poly(A) tail of mRNA in live cells after membrane penetration facilitated by a cell-penetrating peptide and a laser-mediated photoactivation step. The authors demonstrate its applicability in culture as well as in brain tissue to determine the transcriptional profile of single neurons *in vivo*. Similarly, but labelling fully intact cells instead of single-cell molecules, NICHE-seq uses two-photon irradiation to activate photoactivatable green fluorescent protein (PA-GFP) for precise *in situ* labelling of ROIs, followed by fluorescent cell sorting of green cells and subsequent scRNA-seq⁴².

For deterministic selection of ROIs, ZipSeq⁴³ uses optogenetics approaches⁴⁴ with illumination of photo-caged oligonucleotides to serially print barcodes (zip-codes) onto both *in vitro* cell cultures and *ex vivo* tissue sections. DNA oligonucleotides are bound to cells either by cell type-specific antibodies or by membrane lipid

Cluster density
Distance of clusters generated by local clonal oligonucleotide amplification within a sequencing flow cell.

Combinatorial indexing
Multistep split-pool process to index molecules with a unique combination of barcodes for subsequent identification of spatial location (spatial index) or cell identity (single-cell index).

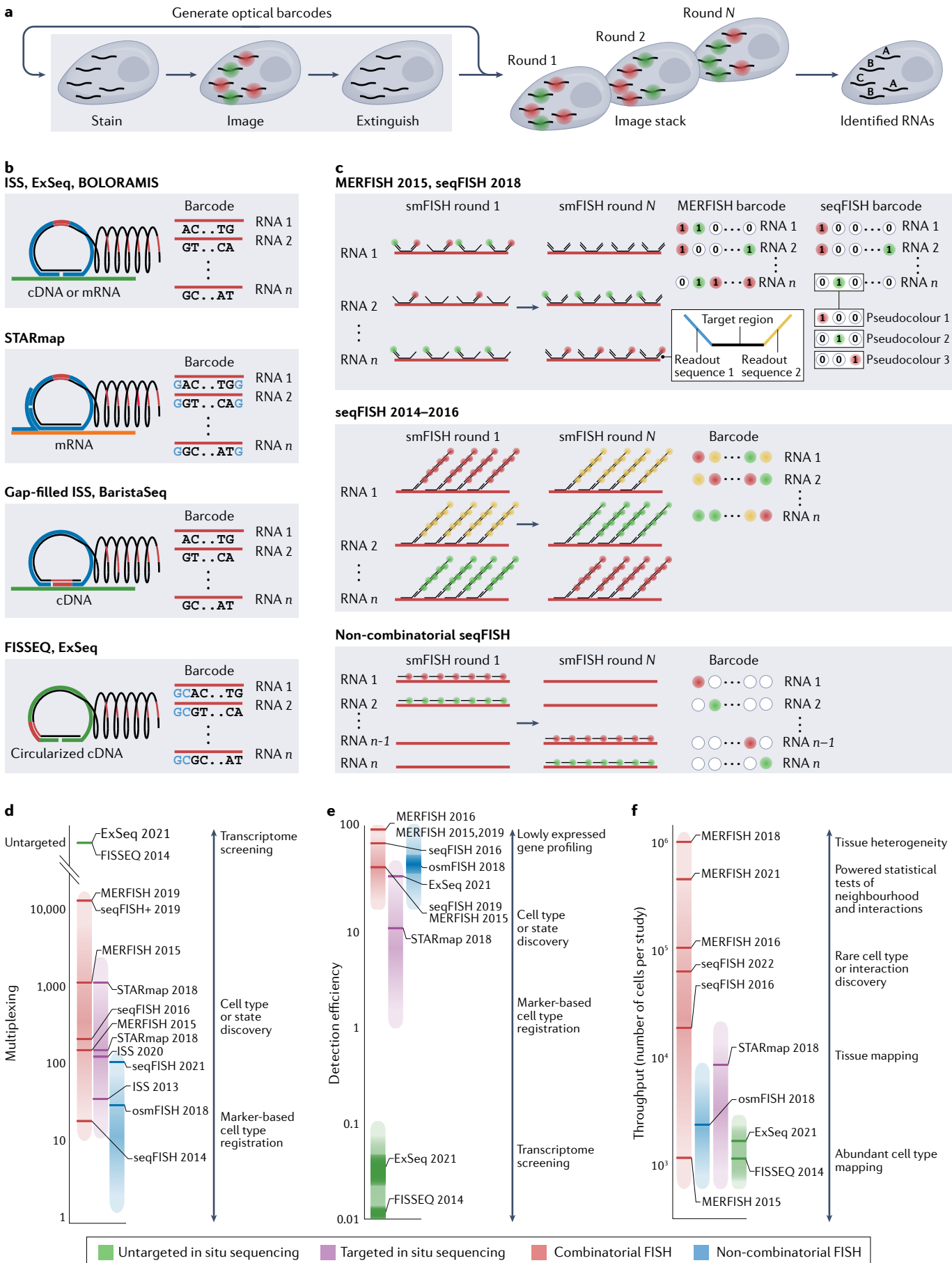


Fig. 3 | An overview of imaging-based spatial transcriptomics methods and their performance. **a** Schematic depiction of the creation of fluorescent signals from individual molecules and the construction of optical barcodes through the repetitive process of single-colour or multicolour fluorescence generation, imaging and signal removal. These optical barcodes can then be used to identify individual RNAs. **b,c** Schematic depiction of the methods that are used to generate optical barcodes and the properties of these barcodes for a selection of *in situ* sequencing-based (part **b**) or fluorescence *in situ* hybridization (FISH)-based (part **c**) methods. With *in situ* sequencing-based methods, fluorescence is generated by the incorporation of fluorescently labelled nucleotides or via ligation of short fluorescently labelled oligonucleotides, that is, sequencing-by-synthesis or sequencing-by-ligation chemistries. The fluorescent patterns, in turn, reveal individual nucleotide sequences, which are, in effect, the barcodes that are used to discriminate different RNAs. Within FISH-based methods, fluorescence is generated by the hybridization of fluorescently labelled oligonucleotide probes and this process can be used to create various fluorescent on-and-off patterns that, in turn, represent barcodes. Multiplexed error-robust FISH (MERFISH) uses binary barcodes to represent RNAs, built from the on-off fluorescent pattern across multiple single or multicolour images. Early sequential FISH (seqFISH) implementations used a colorimetric barcoding scheme, in which each RNA was labelled with one colour in each round. Later seqFISH implementations group multiple imaging rounds to create pseudocolours, in which an RNA is fluorescent in only one image out of the set. The depicted methods should be considered representative but not comprehensive of signal generation and barcoding methods. **d–f** Important performance metrics for image-based transcriptomic methods (distinct colours), including multiplexing (part **d**), detection efficiency (part **e**) and throughput (part **f**). Multiplexing is the number of measurable RNAs; detection efficiency is defined as the fraction of any given molecule actually detected (although we note that methods differ as to the technique used for ground truth, and the listed values and ranges reflect uncertainty in these numbers for different techniques); and throughput is the number of cells characterized by each technique, here estimated by the number of cells reported for individual studies. Different techniques vary in these different performance metrics, which, in turn, shapes the types of biological question (examples listed) that can be addressed. Labelled bars represent a subset of reported studies selected to illustrate the performance range of given techniques and their evolution over time. Importantly, not all metrics are reported for all studies nor are all metrics calculated in the same ways. Therefore, the location of highlighted bars should be considered as approximate estimations of performance, and where numbers are not reported we have estimated a range for these values. ExSeq, expansion sequencing; FISSEQ, fluorescence *in situ* sequencing; ISS, *in situ* sequencing; smFISH, single-molecule FISH; STARmap, spatially resolved transcript amplicon readout mapping.

insertion (for example, lignoceric acid). Spatial labelling is controlled through light-mediated (365 nm) hybridization of barcoded double-stranded DNA to a DNA adapter sequence that is blocked along its length using 6-nitropiperonyloxymethyl (NPOM) conjugated to thymidine. The annealed zipcode terminates in a poly(A) and Illumina Read 2 sequence for streamlined connection to standard scRNA-seq workflows. Sequential washes, patterned illumination and re-hybridization with different spatial barcodes allow multiregional profiling, and fluorophore incorporation allows the enrichment of labelled cells. Variations of ZipSeq use DNA duplex strands bearing an orthogonal NPOM-caged extension to effectively combine zipcode labels. For even more improved scaling and resolution, ZipSeq can add on layers of secondary caged oligonucleotides to exponentially increase the number of definable regions. ZipSeq plugs into scalable droplet-based scRNA-seq workflows to potentially achieve improved molecule coverage compared with ST-based technologies and integration with multimodal readouts.

A different concept to extract spatial transcriptomes underlies NanoString's GeoMx digital spatial profiler, which combines spatial transcriptomes and protein profiling from FFPE or snap-frozen material⁴⁵.

The technology uses photocleavable oligonucleotide tags attached to antibodies or transcriptome-wide RNA hybridization probe sets. ROIs are labelled by UV light triggering the release of multiplexed tags from antibodies or RNA attached to the light-sensitive linker. These tags are simultaneously retrieved from the tissue surface through capillary collection, allowing NGS-based readouts.

Deterministic barcoding in tissue for spatial omics sequencing (DBiT-seq)⁴⁶ allows joint transcriptome and protein profiling, as demonstrated through the analysis of 22 proteins in mouse embryos (similar to scRNA-seq with protein profiling, that is, CITE-seq⁴⁷). The microfluidics-based approach works on formaldehyde-fixed sections on standard glass slides, where parallel microfluidic channels deliver DNA barcodes to the tissue surface to spatially barcode biomolecules *in situ*. Microfluidic chips are clamped onto the tissue slide, and reagents are applied through pipetting into the inlet holes, generating a mosaic barcoding scheme (10, 25 or 50 μm in width). A first barcode is introduced by oligo(dT)-tagged DNA barcodes to initiate *in situ* reverse transcription reaction (horizontal strips). Then, a second chip is applied to the section perpendicular to the first flow direction to ligate a biotinylated second barcode (horizontal strips), unique molecular identifiers and PCR adapters to form 2D mosaic patterning. Spatial precision was estimated by the signal diffusion between channels with 10 μm and 50 μm channels, showing 0.9 μm and 4.5 μm diffusion, respectively. DBiT-seq permits imaging after barcoding to correlate tissue morphology, immunofluorescence signals and spatial omics readouts. After tissue digestion, streptavidin clean-up, template switching and PCR amplification, spatially barcoded transcriptome and protein libraries are prepared for sequencing. After data aggregation of a spatially mapped embryonic day (E) 10 embryo, unsupervised clustering resulted in accurate developmental classification compared with scRNA-seq of E9.5 to E13.5 mouse embryos⁴⁸. Spatially resolved data integrated well with scRNA-seq-derived embryo atlases, allowing for automated cell type annotation based on the reference map.

Image-based spatial transcriptomics

In imaged-based methods for ST, fluorescent signals are generated from individual RNA molecules in their native location and high-resolution fluorescence microscopy is used to detect and distinguish single-molecule signals generated from different RNA molecules. Molecular discrimination is provided by optical barcodes — distinct patterns of fluorescence that are generated through repetitive rounds of fluorescence-signal generation, imaging and signal removal (FIG. 3a). Ultimately, the differences in the growing and exciting array of methods arise in the properties of these optical barcodes and the methods by which they are generated (FIG. 3b,c). These differences, in turn, determine the differential performance of these techniques and the range of biological questions for which different techniques are best suited (FIG. 3d–f). Similar approaches have been developed to profile genomic organization, which we highlight briefly in BOX 1.

Padlock probes

Single-stranded DNA or locked nucleic acid oligonucleotide probes hybridized to a target of interest such that the 3' and 5' ends align on the target molecule, allowing these ends to be ligated to circularize the probe.

Imaging RNA molecules in their native tissue context offers several exciting and complementary benefits compared with the methods described above. For example, high-resolution microscopy offers the ability to resolve the subcellular location of RNAs while tiling images over large sample regions, providing a means to simultaneously map the sub-micrometre-scale intercellular organization of the transcriptome while characterizing both large numbers of cells and centimetre-scale tissue architectures. In addition, by imaging RNAs within their native context, it is sometimes possible to limit RNA loss

(which can arise in NGS-based methods), offering the potential for high detection efficiencies and low detection limits, which, in turn, can allow important sets of functionally relevant but lowly expressed genes to be characterized. Finally, a wide variety of cellular and tissue phenotypes are accessible via optical microscopy, including live-cell dynamics, cellular morphology, genomic organization and modifications, and protein abundance, offering the potential for multimodal characterization of transcriptomic profiles with other biological properties of the sample.

Since their introduction less than 10 years ago, image-based methods for spatially resolved single-cell transcriptomics have moved rapidly from initial proof-of-principle demonstrations to applications that offer windows into a wide range of biological questions, for example, providing insights into gene regulatory modules from co-variation in gene expression⁴⁹, mapping the internal organization of the transcriptome^{49–51}, empowering all-optical screening methods by linking genetic perturbations to synthetic RNA barcodes^{52–58}, inferring aspects of cellular state from RNA-velocity-like measurements of nuclear to cytoplasmic RNAs⁵⁰, or jointly mapping the internal distribution of RNAs and proteins (see Image-based spatial proteomics technologies). However, one of the applications that has attracted much enthusiasm is the use of these techniques to discover cell types and states and map their organization within tissues, effectively creating molecularly defined tissue atlases with cellular and subcellular resolution (FIG. 1d–f and BOX 2). The growing array of image-based single-cell transcriptomic methods can be grouped into two categories, *in situ* sequencing and FISH-based methods, which we summarize here, complementing other contemporaneous reviews^{59–62}. Image-based approaches to ST are evolving rapidly, and although there are many exciting new methods and applications currently on preprint servers, we focus here only on published manuscripts.

Targeted *in situ* sequencing methods. One of the central challenges facing *in situ* sequencing techniques is the generation of specific and bright fluorescent signals from individual molecules. One of the first *in situ* sequencing methods, termed, simply, *in situ* sequencing⁶³ (ISS, hereafter to differentiate it from this class of techniques), introduced a widely adopted solution to this challenge. After *in situ* cDNA synthesis, specificity is provided by padlock probes^{64,65}, where the required ligation of these probes highly favours properly bound probes, and amplification is provided by RCA^{64,66,67}, which replicates one padlock probe into many concatenated copies of that probe, termed a rolling circle product (RCP) or rolonly (FIG. 3d). In ISS, optical barcodes were then generated via sequencing by ligation of a short DNA region unique to each probe. First used to distinguish 39 RNAs in breast cancer slices⁶³, ISS has been extended to the profiling of hundreds of RNAs in brain^{68–72}, spinal cord⁷³, heart⁴, lung⁷⁴ and tumours^{63,75}, and has also been adopted to profile RNA editing⁷⁶ or circular RNA expression⁷⁷.

Although the signals produced by padlock probes and RCA are specific and bright, the fraction of targeted molecules present in the sample that generate a

Box 1 | Image-based methods for mapping the genome

Bulk and single-cell sequencing-based methods, such as the 3C family of methods, have provided tremendous insight into the principles of genome organization over the past decade^{194–196}. However, the contact frequencies produced by these methods provide an indirect measurement of the physical 3D organization of the genome. By contrast, single-molecule fluorescence *in situ* hybridization (smFISH)-based methods offer a direct measurement of spatial organization, and many of the approaches developed for multiplexing smFISH have been co-opted and beautifully extended for the simultaneous identification of a large number of chromosomal loci.

In an early demonstration, tens of distinct chromosomal regions were labelled with FISH probes that leveraged the multiplexed error-robust FISH (MERFISH)-encoding probe design^{197,198}. Sequential readout staining and imaging then revealed, locus by locus, the 3D organization of targeted genomic regions. Subsequent work extended this approach by targeting smaller chromosomal loci and by increasing the ability to resolve labelled loci location and shape using super-resolution microscopy^{197–200}. For example, in optical reconstruction of chromatin architecture¹⁹⁹, microscopy-based chromosomal conformation capture²⁰⁰ or multiplexed imaging of nucleome architectures¹¹⁵ kilobase-scale chromosomal regions were targeted and mapped in *Drosophila* embryos¹⁹⁹ or fetal liver¹¹⁵. Excitingly, in all cases, genomic imaging was coupled with RNA imaging, of one²⁰⁰, tens¹⁹⁹ or ~100 RNAs¹¹⁵, leveraging the RNA barcoding approaches described here.

Combinatorial barcoding has also been co-opted for chromosomal tracing, allowing far more loci to be imaged. For example, both MERFISH and sequential fish (seqFISH) have been used to distinguish genomic loci on the ~1,000-loci scale, allowing the extensive characterization of chromatin across a wide range of length scales from sub-domain structures to trans-chromosomal interactions^{108,117}. Moreover, by including oligo-labelled antibodies and simultaneously targeted RNAs with encoding probes, a single process of sequential readout-probe staining, imaging and signal removal revealed the structure of chromosomal regions, expression of portions of the transcriptome, and the location and abundance of key proteins^{117,221}. These works clearly reveal the potential for image-based multi-omic characterization of single cells within intact tissues.

In parallel, *in situ* sequencing technologies have been introduced for mapping and tracing chromosomal organization. The first methods suite, termed OligoFISSEQ²⁰¹, starts by hybridizing to distinct chromosomal loci DNA FISH probes that contain, like those described above, barcode regions, which are identified via various *in situ* sequencing chemistries or via hybridization or readout probes, as above. Combination with immunofluorescence and multiplexed RNA FISH was also possible with these methods, as was volumetric reconstruction of individual labelled regions via super-resolution microscopy. These approaches have been used to map many tens of loci in cell culture²⁰¹.

In contrast to other genomic tracing methods, the second *in situ* sequencing technology, termed *in situ* genome sequencing¹⁸³, is untargeted and is capable of tagging random genomic loci in individual cells. In this approach, fixed samples are treated with the Tn5 transposase to incorporate priming regions for sequencing into random locations in the genome. These fragments are circularized and amplified via rolling circle amplification. *In situ* sequencing is performed on short unique molecular identifiers (UMIs). Rolling circle products (RCPs) are then removed and sequenced *ex situ* using standard next-generation sequencing approaches, revealing the UMI for each RCP as well as the genomic sequence it contained. The combination of *in situ* and *ex situ* sequencing allows short *in situ* reads and long *ex situ* reads to co-register genomic identity and location but of course requires co-detection of individual RCPs via both modalities.

Box 2 | Applications of image-based spatial transcriptomics in neuroscience

Cellular atlas building is one of the most promising aspects of spatial omics methods. As many of the image-based single-cell transcriptomics methods were first established in the brain, here, we highlight illustrative examples of cellular atlas building in a neuroscience context.

In one early illustrative example, multiplexed error-robust fluorescence *in situ* hybridization (MERFISH)¹⁰⁹ was used to profile the preoptic region of the mouse hypothalamus (FIG. 1d–f). In total, 155 genes were imaged in 1.1 million cells across tens of mice, highlighting the throughput potential of image-based transcriptomics. Single-cell clustering of MERFISH-derived cellular expression profiles matched those of companion single-cell RNA sequencing (scRNA-seq) measurements, confirming that, indeed, targeted measurements can recapitulate cell types and expression profiles. In fact, the increased sensitivity of MERFISH (for any given gene, approximately sevenfold more copies per cell were observed in MERFISH relative to scRNA-seq) allowed the discovery of cell type divisions, defined, in part, by lowly expressed neuropeptide and hormone receptors, not found by scRNA-seq, illustrating the discovery potential offered by the high detection efficiency of image-based methods. The inclusion of an activity-dependent gene further allowed cell types to be associated with specific hypothalamic circuits.

In another illustrative example, *in situ* sequencing via spatially resolved transcript amplicon readout mapping (STARmap)⁷⁹ was similarly used to identify cell types, map their spatial organization and provide functional annotations in the mouse primary visual and prefrontal cortex. This work illustrated the ability of image-based methods to provide deep functional insight into the transcriptional response of different cell types by including a panel of genes with activity-dependent transcription. Moreover, this study addressed a crucial question for targeted methods. Namely, how many genes are required to capture cell type diversity? Extending STARmap to 1,020 from 160 genes increased the number of defined cell types in the visual cortex only modestly, from 12 to 15 types. Clearly, the number of appropriate genes for cell type discovery will be gene and tissue dependent, yet this study and the MERFISH¹⁰⁹ work provide support for the notion that thousands of genes may be unnecessary for cell type definition in some cases. Finally, the authors demonstrated one of the potential strengths of image-based methods—the ability to extend to three dimensions. By leveraging a non-combinatorial barcode to profile 28 genes in 30,000 cells from 150 µm-thick samples of the visual cortex, the authors revealed spatial

clustering in inhibitory neuron types that was not apparent in the 8 µm-thin sections.

In another recent MERFISH study of the mouse motor cortex¹¹⁰—part of the larger, multi-laboratory, multimodal motor cortex atlas²⁰² driven by the BRAIN Initiative Cell Census Network (BICCN)—the authors profiled 258 genes in the mouse motor cortex, measuring ~300,000 cells in two adult mice. These measurements defined the expected complexity in the motor cortex, again producing measurements in high concordance with scRNA-seq and cementing the notion that targeted panels have cell type discovery potential that is comparable to that of untargeted measurements. Interestingly, owing to the ability to precisely define the location of each cell within individual cortical layers, MERFISH was able to link subtle variations in gene expression to tissue location or cellular neighbourhood, a key promise of spatial transcriptomic methods. Finally, this work also exemplified the ability of image-based methods to overlay transcriptional information onto the wide variety of image-based characterization methods that already exist. Performing MERFISH and fluorescent imaging in mice in which three distinct fluorescent retrograde tracers had been injected into three different brain regions not only revealed the transcriptional identity of each neuronal cell type in the motor cortex but also allowed detailed mapping of their project patterns to these three brain regions.

Illustrating the multi-omic potential of image-based methods, Cai and colleagues¹²¹ combined image-based proteomics, transcriptomics and genome tracing to characterize the correlates of nuclear organization in cells of the mouse cerebral cortex with sequential FISH (seqFISH). The mapped organization of the 3D genome agreed well with sequencing-based measurements (Hi-C) and recapitulated the known compartmentalization of chromatin states. First seen via chromatin tracing with MERFISH in cell culture²⁰³, this work further demonstrated that, in tissue, topologically associated domain boundaries, which emerge clearly in population average, are far less defined at the single-cell level. Finally, by leveraging RNA and genomic structure information, the authors could show that distinct cell types have distinct nuclear organization, which suggested that the organization of chromosomes around nuclear bodies and regions of distinct chromatin marks correlates with the differential gene expression of different cell types. These and other highly multiplexed, multimodal measurements^{108,117} raise the possibility of new mechanistic insights into the determinants of genome organization and its consequences for genome maintenance, replication and expression.

Detection efficiency

Capacity to capture or label RNA, DNA or protein molecules to allow subsequent quantification.

SNAIL probes

Probes that contain a primer probe and a padlock probe, both of which hybridize to the same RNA, placing both probes in proximity such that the 3' and 5' end of the padlock can hybridize to the primer probe, allowing the circularization of the padlock via DNA-templated ligation.

Expansion microscopy

An effective super-resolution optical microscopy technique that increases effective optical resolution by attaching the signal of interest to a charged hydrogel that is then physically and isotropically expanded.

detectable signal—that is, the detection efficiency—was modest for ISS (the exact value was unreported, but is likely in the order of ~5%)⁶³. One possible reason for the low detection efficiency could be the low efficiency of *in situ* cDNA synthesis. As cDNA synthesis was used to allow DNA-templated ligation of padlocks, BOLORAMIS⁷⁸ introduced one potential solution by using an RNA-templated DNA ligase, SplintR ligase, which increased detection efficiency to ~20% and allowed profiling of ~100 RNAs in neuron-microglial cell culture.

Spatially resolved transcript amplicon readout mapping (STARmap)⁷⁹ introduced another approach to bypass cDNA synthesis with a two-component padlock-probe variant termed SNAIL probes⁷⁹. The key insight was the use of a second supporting probe for each padlock, which provided a DNA template for padlock ligation. Optical barcodes were then built from a short DNA sequence unique to each targeted RNA with a novel sequencing-by-ligation approach termed SEDAL sequencing⁷⁹ that allowed the detection of one corrupted barcode element. STARmap has been used to map hundreds to around one thousand different RNAs

in cell culture^{79,80}, mouse brain⁸⁰, placenta⁸⁰, gut⁸⁰ and cardiac organoids⁸⁰ with a reported detection efficiency of ~10%⁷⁹.

The crowded cellular environment may also challenge *in situ* enzymatic steps. To address this challenge, targeted expansion sequencing (ExSeq)⁸¹ combines expansion microscopy^{82,83} with *in situ* sequencing by anchoring RNAs to an expandable hydrogel, removing cellular components and expanding the gel before binding, ligating and amplifying padlock probes, and using sequencing-by-ligation to generate optical barcodes. Targeted ExSeq has been used to detect tens to hundreds of genes in the mouse primary visual cortex, hippocampus and human metastatic breast cancer biopsy samples, with ~40% detection efficiency⁸¹. Coupling *in situ* sequencing to expansion microscopy offers the additional benefit that RNAs can be registered with other cellular features at sub-diffraction-limited resolution.

In each of the targeted methods above, the RNA is identified by a short synthetic barcode on the padlock. However, there are instances where it is useful to directly measure the sequence of short portions of the targeted RNA. Gap-filled ISS⁶³ addresses this need by separating

Combinatorial barcoding

This process involves the use of barcodes in which the value of individual barcode elements, e.g. '1' values in individual bits of binary barcodes, are shared between multiple targets with targets discriminated by the unique combination of barcode elements, e.g. '101' versus '110'.

Error-robust and correcting barcoding schemes

Barcode schemes in which extra barcode elements are added that allow the detection of barcode elements corrupted in the measurement process and, for some errors, the identification of the correct value for the corrupted element.

the hybridization sites for the 5' and 3' ends of the padlock and using a gap-filling polymerase to fill this gap, effectively copying this portion of the target molecule into the sequence of the padlock. Selective ligation of complementary short oligos can also fill the gap⁸⁴. Gap-filled ISS has been used to distinguish oncogenes in breast cancer samples⁶³ and extended to 12 nt regions to empower all-optical pooled CRISPR screening⁵⁸. Gap-filled ISS has also been recently extended with BaristaSeq⁸⁵, in which improved gap-filling enzymes were used to increase colony production efficiency, and used in BARSeq⁵⁶ or BARSeq2 (REF. ⁵⁷) to map the projections of neurons uniquely marked by synthetic RNA barcodes.

Untargeted *in situ* sequencing methods. *In situ* sequencing can also be performed in an untargeted fashion by using the sequence of the RNA itself to generate the optical barcode. The first method to take this approach was fluorescence *in situ* sequencing (FISSEQ)^{86,87}. FISSEQ begins with an *in situ* cDNA synthesis reaction, and then short cDNA fragments are circularized to produce an RCA template. Incorporation of a common priming region during the circularization allows the production of colonies and provides a sequence from which to prime sequencing-by-ligation chemistry. FISSEQ has been used to detect thousands of different transcripts and distinguish splice variants within human cell culture⁸⁶.

The ability to directly identify RNAs from their sequence promises many benefits, including untargeted detection of RNAs, splice junctions or single-nucleotide variations (SNVs); however, the required *in situ* enzymatic reactions and chemistries seem to be relatively inefficient: less than 0.01% of the RNA content of the cell is detected with the FISSEQ protocol^{78,86,87}. Untargeted ExSeq⁸¹ combines modified FISSEQ protocols with expansion microscopy to improve efficiency. Detection efficiency is also increased by reducing *in situ* sequencing read length. *In situ* reads are long enough (20 nt) to be unique among all measured RCPs but perhaps too short to uniquely identify some RNAs. However, RCPs are then captured and subjected to longer-read *ex situ* sequencing, which registers *ex situ* and *in situ* reads, providing unambiguous RNA identification and defining features such as splice junctions or SNVs while simultaneously re-registering *ex situ* reads in space. Untargeted ExSeq has been used to profile gene expression in the mouse brain, *Caenorhabditis elegans*, *Drosophila* embryos and cell culture, with improved but still modest detection efficiency (also unreported)⁸¹.

Fluorescence *in situ* hybridization methods. In FISH, individual RNA or DNA molecules are labelled by hybridizing them to fluorescently labelled oligonucleotides of complementary sequence. When coupled with bright fluorophores and tens of unique probes per RNA, the signal from individual RNA molecules can be robustly observed as diffraction-limited spots, allowing individual molecules to be localized and counted. This approach, termed smFISH^{88,89}, is the gold standard for gene expression and spatial distribution measurements in fixed cells. However, smFISH multiplexing has

historically been modest, limiting transcriptome-scale investigations with this powerful technique to massively parallel, single-plex screens⁹⁰. Early multiplexing efforts focused on using different colours of fluorophores with colorimetric combinatorial barcodes to identify RNAs, but were limited to tens of RNAs^{91–94}. Exchanging colorimetric barcodes for sequential barcodes, built through successive rounds of smFISH, was a key insight that allowed substantial expansion in the multiplexing of smFISH. This concept was developed and introduced in parallel by two techniques: sequential FISH (seqFISH)⁹⁵ and multiplexed error-robust FISH (MERFISH)⁴⁹.

In a first proof of principle, seqFISH⁹⁵ identified 12 different RNAs by staining samples with probes that assigned each RNA one of four colours. The sample was imaged to determine the colour assigned to each RNA; FISH probes were removed by digestion; and the sample was re-stained to assign each RNA a second of the four colours. Thus, individual RNAs could be discriminated by the $4^2 = 16$ possible two-colour optical barcodes (FIG. 3c).

In parallel work, MERFISH showed that this concept could be used for transcriptome-scale profiling, characterizing ~100 or ~1,000 RNAs in cell culture⁴⁹. Individual RNAs were assigned a binary barcode, and a set of DNA-encoding probes was created to imprint representations of these barcodes onto target RNAs via *in situ* hybridization (FIG. 3c). Barcodes were represented via a unique combination of readout sequences, with one readout sequence assigned to each bit, and the presence or absence of that readout representing a '1' or '0', respectively. The sample was stained with encoding probes and then with a fluorescently labelled readout probe complementary to a readout sequence, imaged and the signal removed with photobleaching⁴⁹ or, in later protocols, chemical removal⁹⁶. By repeating this readout-probe staining process, the presence or absence of fluorescence in each smFISH image revealed the barcode for each targeted molecule, bit by bit⁴⁹ (or in groups of bits when multicolour imaging was used^{96,97}).

While combinatorial barcoding allows the rapid generation of massive numbers of unique barcodes, barcoding capacity was not the only challenge to transcriptome-scale multiplexing. First, rare smFISH measurement errors compound quickly in combinatorial barcodes, severely limiting measurement accuracy. First introduced with MERFISH⁴⁹, error-robust and correcting barcoding schemes have become a widely adopted solution to this challenge^{51,98–100}. Second, slow probe hybridization to cellular RNA can also challenge long-barcode readout with direct RNA labelling^{95,98}. As readout-probe binding to readout sequences is orders of magnitude faster^{49,96}, the two-step hybridization process — with one slow hybridization effectively imprinting barcodes on RNAs, followed by a series of fast readout hybridizations to determine barcodes — has also become a standard solution^{51,98–100}. Third, smFISH typically leverages tens of probes per RNA to provide binding redundancy and signal amplification; unfortunately, standard synthesis of the tens to hundreds of thousands of unique probes required to target thousands of RNAs would be prohibitively expensive. Building on the pioneering oligopaints protocol for DNA

Oligopools

Collections of tens to hundreds of thousands of unique, custom oligonucleotide sequences generated inexpensively but in small quantities by array-based methods.

Pseudocolours

Collections of images in which each molecule is fluorescent in only one image with that image representing the pseudocolour, i.e. n pseudocolours can be thought of as n -bit barcodes in which only one bit contains a '1'.

Hybridization chain reaction (HCR). An amplification approach in which two meta-stable, fluorescently labelled DNA hairpins are used to polymerize a repeating structure from these hairpins.

Branched DNA amplification

(bDNA). An amplification approach that leverages a DNA oligonucleotide 'amplifier' that contains a targeting sequence in combination with multiple copies of a secondary binding site, effectively amplifying fluorescent signals by converting one binding site into multiples. Iterative rounds of amplification are possible.

FISH probe construction¹⁰¹, MERFISH^{49,102} introduced a widely adopted^{51,98,99} high-yield protocol to inexpensively amplify such probes from complex, custom oligopools¹⁰³.

Nevertheless, arguably the greatest challenge to the highest degree of multiplexing is RNA density. To define optical barcodes, the signals from individual RNAs must be spatially resolved, which becomes more challenging as the number of RNAs and, thus, the labelled RNA density, increases. The use of signal absence to denote a barcode element (for example, no fluorescence represents '0'), as introduced with MERFISH⁴⁹, provides one solution, as the number of '1' bits can be fixed and signals diluted across more images by increasing the length of barcodes. The generalization of colorimetric barcodes to barcodes based on pseudocolours by the seqFISH^{51,99,104} team leverages this insight (FIG. 3c). Similarly, the RNAs themselves can be physically diluted with expansion microscopy^{82,83}, as demonstrated with MERFISH^{50,105}.

By leveraging these advances, transcriptome-scale measurements are now possible: the seqFISH team has measured ~10,000 sites of nascent transcription⁹⁹ or RNAs in cell culture and mouse brain⁵¹ in a protocol termed seqFISH+, and MERFISH was used to measure ~10,000 RNAs in cell culture⁵⁰. Crucially, these measurements were made with high detection efficiency in cell culture (50% for seqFISH+ (REF.⁵¹) and 80% for MERFISH⁵⁰). Targeting hundreds to thousands of genes, MERFISH has been used to profile gene expression in cell culture^{49,50,96,97,105–108}, brain^{97,109–112}, glioblastoma¹¹³, fetal liver^{114,115} and gut¹¹⁶, and to measure synthetic RNA barcodes, empowering all-optical pooled screening^{52,53}. Similarly, seqFISH and its recent variations have been used to profile gene expression in cell culture^{95,99,117}, dissociated lymphocytes¹¹⁸, brain^{51,98,119–122} and mouse embryo¹²³.

Another challenge that FISH-based methods face is fluorescence background. To overcome sample auto-fluorescence, FISH-based methods have turned to signal amplification: seqFISH was combined with hybridization chain reaction^{98,124}, and MERFISH was combined with branched DNA amplification¹⁰⁶. In parallel, FISH-based readout of optical barcodes has been combined with RCA by leveraging padlock probes for the encoding probes in HybISS¹⁰⁰. Additional forms of smFISH amplification, such as SABER¹²⁵ and clampFISH¹²⁶, could be attractive amplification methods. The nonspecific binding of FISH probes is another source of background that becomes increasingly important as the number of genes and, thus, FISH probes, increases. Binding to non-RNA cellular components is a major source of such background, which the MERFISH team solved with matrix embedding and clearing⁹⁷. Inspired by expansion microscopy⁸², this more widely adopted and modified protocol⁵¹ anchors RNAs to an embedding hydrogel film and then digests all unneeded cellular components to remove off-targets for FISH. In parallel, split-FISH¹²⁷, HybISS¹⁰⁰, SCRINSHOT¹²⁸ and PLISH¹²⁹ reduce such background by generating detectable fluorescence only if pairs of probes bind adjacently on each RNA (split-FISH), padlock probes can be ligated (HybISS/SCRINSHOT) or a combination of both approaches (PLISH). Together split-FISH, HybISS/SCRINSHOT and PLISH have been used to characterize

tens to hundreds of genes in brain^{100,127,130,131}, kidney¹²⁷, ovaries¹²⁷, liver¹²⁷, lung^{128,129} and trachea¹²⁸.

In parallel, there are biological questions for which the measurement of hundreds or more genes is not necessary, and several groups have introduced non-combinatorial methods that leverage sequential rounds of smFISH to identify RNAs, with each colour channel in each round of imaging associated with a single RNA (FIG. 3c). Multiplexing ranges from ~10 to ~100 RNAs. Examples of such methods include osmFISH¹³², ExFISH⁸³, clampFISH¹²⁶, par-seqFISH¹³³, EASI-FISH¹³⁴, spatial genomic analysis (SGA)¹¹⁹ and contemporaneous unnamed methods¹³⁵. The major advantage of these methods is that RNA density does not pose the same challenge for these methods, as dense signals from one RNA cannot corrupt those of a different RNA. Indeed, this approach has been routinely combined with combinatorial barcoding to allow some of the most highly expressed genes to be included in these measurements^{98,109,110}.

Advanced computational approaches can also infer RNA abundance from images in which individual RNAs are not resolved. For example, in corrFISH¹³⁶, spatial correlations are used to extract the abundance of RNAs assigned combinatorial barcodes. In parallel, in compressed sensing approaches¹³⁷, machine-learning-based methods are used to reconstruct the abundance of RNAs from measurements of the total fluorescence signal generated by specific combinations of RNAs measured in each round.

Image-based spatial proteomics technologies

In imaging-based methods for spatial proteomics, signals are generated from proteins in their native in situ location through specific targeting by antibodies. Although most methods for spatial proteomics are similar in principle, differences emerge in the approach to visualization and discrimination of the antibodies, as well as properties for signal amplification. These differences, in turn, determine the range of biological questions for which different techniques are best suited.

Imaging proteins in their native tissue context offers many complementary advantages compared with transcriptomics methods. Similar to the image-based ST methods, there are many advantages of using an imaging-based readout, including possibilities to map the subcellular distribution of proteins while tiling images to map large tissue regions and a high number of cells. Also, access to the wide variety of cellular and tissue phenotypes that are accessible via optical microscopy provides ample opportunities for multimodal biological applications, as outlined in the preceding section.

Whereas ST methods offer significantly higher multiplexing and provide detailed insights into cell types and their gene expression patterns, spatial proteomics technologies are limited in their multiplexing capabilities (currently around 50–100 proteins) but offer other advantages. For example, protein levels serve as a better proxy for cellular activity, and it is well known that RNA levels do not always correlate with protein levels¹³⁸. Also, some proteins are very stable, whereas the corresponding RNA levels can be very low and difficult to detect

with transcript-based methods. Other advantages of detection at the protein level include precise subcellular localization to organelles, studies of the extracellular environment and its impact on tissue architecture, and detection of specific proteoforms or post-translational modifications such as phosphorylation. For these reasons, spatial proteomics methods offer unmatched opportunities to map cell states, signalling activity and cell–cell interactions, as well as higher order spatial organization. For example, several spatial proteomics methods have been applied to study the structured organization of the tumour–immune microenvironment of breast cancers^{139–141}.

The methods for image-based spatial proteomics are in general applicable to both fresh-frozen and FFPE samples and can be grouped into two categories: cyclic fluorescent approaches and one-step mass-tag approaches. For details on subcellular spatial proteomics methods based on cell fractionation¹⁴² and mass spectrometry imaging^{143,144}, we refer readers to other reviews. All these methods rely on image alignment, cell segmentation and downstream spatial analysis, as reviewed elsewhere.

Targeted highly multiplexed antibody-based imaging methods. To study the expression of proteins *in situ* with single-cell or even subcellular resolution, highly multiplexed imaging methods have recently been developed. These methods take off from classical immunohistochemical (IHC) or immunofluorescent (IF) strategies whereby proteins of interest are visualized through specific antibodies, as developed already in 1941 (REF.¹⁴⁵). There is a plethora of such highly multiplexed methods and the key difference between them is that they employ different detection strategies to overcome the spectral limitations of conventional fluorescence microscopy and thus allow simultaneous probing of typically 20–60 proteins in FFPE or fresh-frozen tissue samples¹⁴⁶. Highly multiplexed antibody-based imaging methods can be classified on the basis of the mode of antibody tagging and visualization technology. The antibody tagging can be based on either fluorophores, DNA barcodes, enzymes or metal tags, whereas the visualization strategy is commonly fluorescence imaging or mass spectrometry (reviewed in REFS. ^{147–149}). These differences are what provides the methods with their respective advantages and disadvantages and are important to consider for different biological applications.

Crucially, all these methods rely on the use of antibodies, which poses limitations and makes antibody validation key to obtaining reproducible and accurate results¹⁵⁰. For regular IHC experiments, antibodies are normally validated in terms of specificity, often using a negative and positive sample, but other approaches such as paired antibodies, immunoprecipitation and gene silencing are available¹⁵¹. As antibody performance can differ based on the context of its usage, including the type of tissue used, experimental parameters such as antigen retrieval protocols are commonly optimized for each sample (for example, pH, heat treatment and buffer composition). This is where multiplexed antibody-based imaging applications encounter additional constraints, as all antibodies need to work under identical conditions.

As DNA conjugation can interfere with antibody function, this requires further validation to ensure that antibody specificity is maintained and that the oligo can be properly detected. Therefore, one needs to be aware of the particular considerations required for preparing antibody panels for multiplexed experiments, as reviewed in detail elsewhere¹⁴⁶. In addition to different strategies for visualization, there have been developments for improved tissue preservation and uniformity of staining across many cycles using tissue clearing techniques^{152–156} (reviewed in REF.¹⁵⁷). In summary, the performance of these methods is limited by the antibodies used in them; although many methods have used the same antibodies, often targeting immune cells, we are likely to see more differentiation as the pool of antibodies validated for multiplexed use continues to grow.

Cyclic fluorescent approaches. Similar to image-based ST methods, fluorescence-based spatial proteomics approaches achieve multiplexing by adopting some version of a cyclic protocol that circumvents the issue of fluorescence spectral overlap. It generally includes the following steps: first, immunostaining with oligonucleotide or fluorescently labelled antibodies; second, fluorescent image acquisition, either directly or after addition of fluorescently labelled complementary oligonucleotides; and third, fluorophore inactivation or removal of hybridized oligonucleotide probes or bound antibodies.

The first group of fluorescent cyclic approaches employ a cyclic strategy of ‘staining–imaging–bleaching’ or ‘antibody removal’ using either fluorescently labelled primary antibodies (direct immunofluorescence) or secondary antibodies (indirect immunofluorescence). Key considerations for such cyclic methods relate to tissue degradation, proteome loss and epitope destruction due to the stress of repeated fluid exchanges, as well as incomplete fluorophore removal between cycles. Direct methods include SWITCH¹⁵⁴, multiplexed immunofluorescence (MxIF¹⁵⁸), tissue-based cyclic immunofluorescence (t-CyCIF^{159,160}) and iterative bleaching extends multiplexity (IBEX¹⁶¹). These methods mainly differ in the way that the fluorescence signal is removed and basically represent incremental developments that allow more efficient bleaching while minimizing tissue destruction and protein degradation. MxIF is based on chemical bleaching (alkaline oxidation chemistry) to eliminate cyanine-based dye fluorescence. t-CyCIF further developed this to a combined chemical and light bleaching protocol (hydrogen peroxide, light and high pH) compatible with Alexa dyes. IBEX introduced lithium borohydride to bleach fluorophores in a short time, thus reducing the overall cycling time to better preserve the tissue and allow up to 20 iterative cycles. Iterative indirect immunofluorescence (4i¹⁶²) uses an indirect approach whereby the primary antibodies are visualized with fluorophore-labelled secondary antibodies. By introducing a novel buffer to prevent covalent light-induced crosslinking of the fluorophores to the tissue sample, a cyclic approach of antibody staining, imaging and antibody elution can be used. An advantage with using secondary antibodies is that no antibody conjugation is needed, making the method more applicable to a variety of biological applications.

using off-the-shelf available antibodies. Another advantage includes the signal amplification obtained owing to multiple secondary antibodies binding each primary antibody. Cyclic methods often employ autofluorescence registration between cycles for computational subtraction to improve the signal to noise ratio, and recent work has demonstrated feasibility of 21 iterative cycles without significant tissue destruction¹⁶³. Key considerations in cyclic methods relate to maintaining tissue integrity and optimizing the order of antibodies in the cycles to ensure optimal detection of each epitope.

Early work exploring such approaches allowed visualization of 10–20 target proteins in cultivated cells^{164,165}, whereas current methods routinely allow multiplexing of more than 60 target proteins in a tissue section and have been used to study tissue architecture, tumour heterogeneity and states of signal transduction networks.

The second group of fluorescent cyclic approaches is based on DNA barcoding of antibodies. These methods were also developed to circumvent the spectral limitations of fluorescence, with the advantage that they provide faster cycling than the bleaching protocols mentioned above. They overcome the speed restrictions by allowing for a single round of immunostaining, followed by sequential readout of the DNA barcodes by rapid binding and unbinding of fluorescent imager strands using DNA-exchange imaging (DEI¹⁶⁶), *in situ* polymerization of fluorescent dNTP analogues using co-detection by imaging (CODEX^{167,168}) or by DNA concatemers in signal amplification by exchange reaction (immuno-SABER¹⁶⁹), offering programmable signal amplification without *in situ* enzymatic reactions. The main advantage of these methods is the simple one-step immunostaining, which leads to faster assays and fewer issues with sample loss and epitope destruction given that all antibodies are bound in one step. Drawbacks include the need to make and validate antibody–oligo conjugates. Of these methods, CODEX is by far the most applied to date, likely owing to the commercial availability of an automated instrument for the cyclic imaging as well as validated antibody panels.

The dynamic range of the cellular proteome approaches seven orders of magnitude and ranges from one to ten million copies per cell¹⁷⁰. To visualize low-abundance proteins, such as certain transcription factors or phosphorylated signalling proteins, signal amplification is essential. Amplification methods, such as immuno-SABER¹⁶⁹, immunosignal hybridization chain reaction^{171,172} and enzymatic amplifications such as horseradish peroxidase¹⁷³ or tyramide signal amplification (TSA)¹⁷⁴ approaches can improve the signal to noise ratio. Until recently, TSA methods such as Opal IHC have been restricted to simultaneous detection of up to eight proteins as the tyramide-linked fluorophores remained bound to the tissue despite antibody removal. Recent advances in the development of the IBEX protocol have shown that lithium borohydride can be used to eliminate the signal from several Opal dyes, providing a means for the highly multiplexed imaging of low-abundance proteins in heavily fixed and autofluorescent tissues¹⁶¹. With the dynamic range of the human proteome being significantly higher than

that of fluorescence microscopy, all these methods will require careful consideration of how best to design antibody panels and iterative cycles to allow visualization of targets with both high and low abundance.

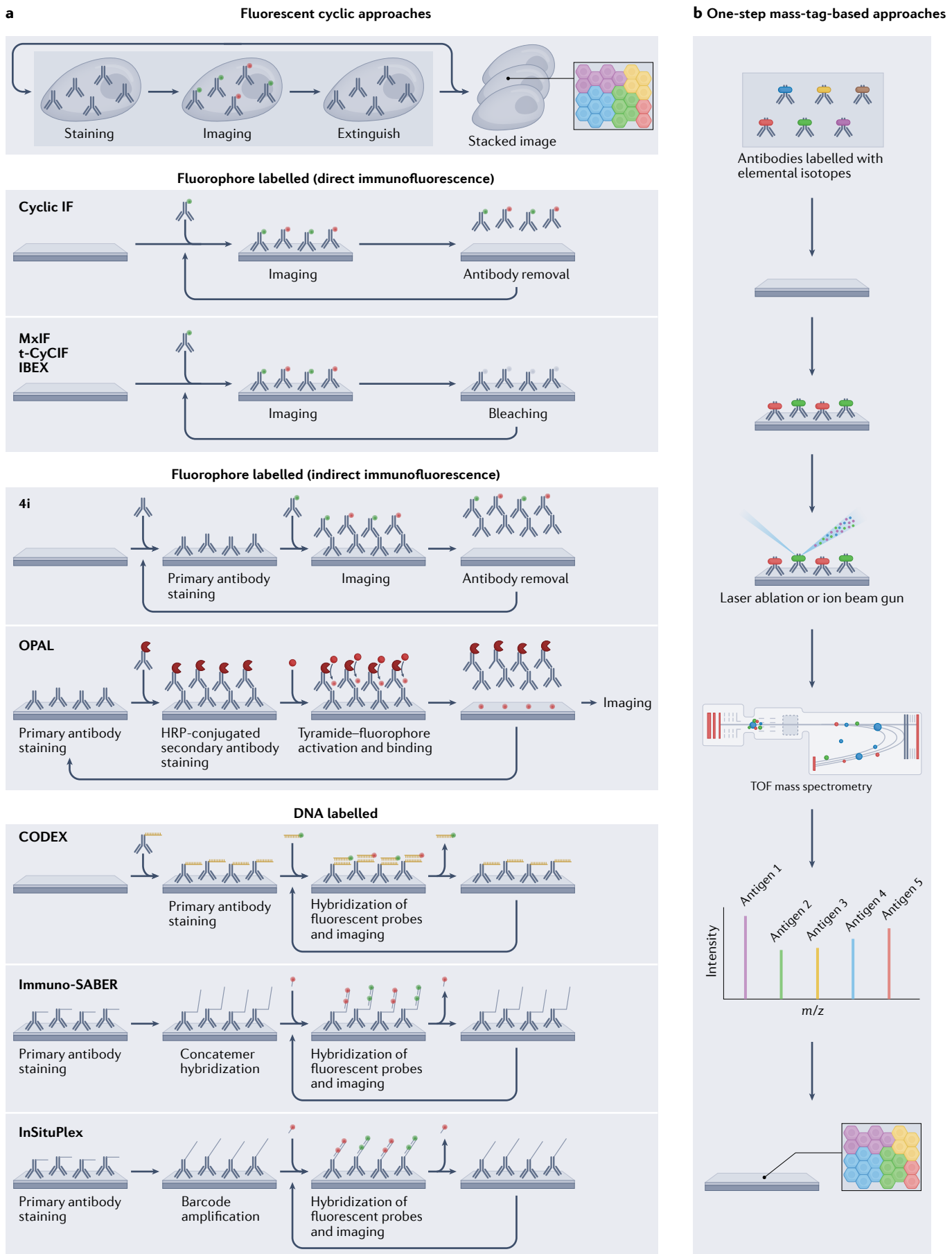
Exciting developments in this space include multi-omics methods for simultaneous image-based ST and proteomics, whereby RNA detection maps cell types while protein detection maps the extracellular matrix and specific cell states, for example.

One-step mass-tag-based approaches. A separate group of methods represent a ‘one-step approach’ in which the capture of multiparametric data is performed without cyclic imaging, thus avoiding all the crucial issues of tissue destruction owing to the many cycles and focus drifting between cycles. In these methods, antibodies are conjugated with ionizable metal mass tags (mostly from the lanthanide series) and mass spectrometry is used for readout (FIG. 4). These methods allow visualization of more than 40 proteins in a tissue section based on one-step immunostaining and one-step detection. Examples of such methods are multiplexed ion beam imaging (MIBI^{139,175}) and imaging mass cytometry (IMC¹⁷⁶). In IMC, the tissue is ablated with a laser with a 1 µm spot size, which rasterizes over the selected region of interest, where tissue is then aerosolized, atomized and ionized, and fed into a time-of-flight mass spectrometer for analysis of isotope abundance. In MIBI, an oxygen duoplasmatron primary ion beam rasterizes over the tissue, ablating a thin layer of the tissue surface, liberating antibody-bound metal isotopes as ions. These secondary ions are fed into a time-of-flight mass spectrometer for analysis of isotope abundance. In both IMC and MIBI, the isotope abundance of each spot can be mapped back to the original coordinates, producing a high-dimensional image qualitatively similar to a fluorescence microscopy image. A key advantage is the robustness of the one-step approach, the high dynamic range (quantification over a five-log dynamic range¹⁷⁵), and low background signals (that is, no issues with autofluorescence). Unlike for the other fluorescence-based approaches, the samples must be vacuum stable, and antibody signals cannot be amplified¹⁴⁶. Both IMC and MIBI also require specialized instrumentation that is expensive and not readily available to most labs.

Exciting new developments include high-definition MIBI (HD-MIBI), which allows multiplexed imaging in three dimensions of both targeted proteins and exogenously added structurally unmodified small molecules with resolution down to 30 nm¹⁷⁷. The authors demonstrated the power of this novel method by mapping the chemotherapy drug cisplatin with proteins in various subnuclear structures and showed that selective subcellular drug relocalization may modulate resistance to this important chemotherapeutic agent.

Future perspectives

The promise of spatial profiling is clear, and past and continued improvements in resolution, sensitivity, multiplexing, throughput and access have resulted in the broader implementation of these respective technologies for basic research, such as neuroscience and



◀ Fig. 4 | An overview of imaging-based spatial proteomics methods. Methods can roughly be classified into two main approaches: ‘fluorescent cyclic approaches’ or ‘one-step mass-tag-based approaches’. **a** | Schematic depiction of fluorescent cyclic approaches and the creation of fluorescent signals from individual proteins through the repetitive process of single or multicolour fluorescence generation, imaging and signal removal. There are versions of this approach that differ in the methodology for fluorescence visualization and removal, including the use of direct immunofluorescent methods with fluorophore-labelled antibodies, indirect methods with fluorophore-labelled secondary antibodies and methods that use DNA-conjugated antibodies. **b** | Schematic depiction of one-step mass-tag-based approaches in which antibodies labelled with ionizable metal mass tags are used for labelling. The tissue is ablated with a laser or ion beam, liberating antibody-bound metal isotopes as ions for subsequent detection using time-of-flight (TOF) mass spectrometry. 4i, iterative indirect immunofluorescence; HRP, horseradish peroxidase; IF, immunofluorescence; MxIF, multiplexed immunofluorescence; m/z , mass to charge ratio; t-CyClF, tissue-based cyclic immunofluorescence.

developmental biology, or translational efforts in the area of cancer or autoimmune disorders. Especially for translational research and in the clinic, spatial profiling has already been standard practice for decades through histopathology assessment for disease diagnosis and treatment decision. However, current pathology methods rely greatly on the manual assessment of cell and tissue structure (mostly through H&E tissue staining) and modestly multiplexed marker measurements. Established features have enough discriminative power to distinguish healthy from diseased tissue and, thus, are often sufficient for broad diagnostic purposes. However, measures of tissue morphology alone lack the molecular depth promised by this new toolbox of ST, proteomic and genomic techniques, combining deep molecular and spatial profiling to better predict patient prognosis or the success of therapeutic intervention. The spatial omics technologies reviewed here have the potential to transform current pathology practice into high-precision readouts through the digitalization of molecular profiles and the associated increase in the feature space by orders of magnitude. However, to achieve its transformative potential many aspects of this field must continue to mature.

Data and performance standards. A key requirement on the roadmap towards broad use and clinical implementation will be the standardization of data generation and file formats¹⁷⁸ through automation and consistent processing pipelines¹⁷⁹. Not only will such standards continue to drive computational innovations, they would also facilitate the large-scale integration of spatial omics and existing pathology imaging data. In turn, this may promise the ability to extract crucial insights from routine or lowly multiplexed images, reducing profiling requirements back to standard imaging, minimizing costs, facilitating accessibility and, ultimately, democratizing health care. Indeed, such a reductionist approach has been successful with H&E using computational histopathology¹⁸⁰ and contrast-enhanced CT¹⁸¹ images for features such as immune cell infiltration or association with genomic and transcriptional aberrations.

Standardization of performance metrics and standards for the reporting of such quality control metrics will also be an essential step to maintain the rate of development and adoption of these profiling tools. For example, quantities such as the fraction of captured or

detected molecules (capture or detection efficiency), or antibody validation data, are crucial metrics for comparing technologies and judging the proper technology for a specific set of questions. Yet, there are no commonly agreed-upon methods for quantifying such values, nor is it generally accepted that such values need to be reported. For example, current high-resolution spatial indexing technologies have much lower molecule capture rate per unit than lower-resolution methods, but their systematic comparison is impeded by the lack of standardized performance metrics. This includes the absence of standard samples and targeted gene or protein sets, which could greatly facilitate cross-modality comparisons. Similarly, among the image-based transcriptomics methods, detection efficiency is most often measured relative to single-plex smFISH of the same RNA in matched samples, but other metrics, such as comparison with scRNA-seq, are also used, or in some cases no measurements are provided. Given the ease with which smFISH can be performed in a range of samples, we encourage the field to adopt this common benchmark for estimating RNA capture or detection efficiencies for all ST methods.

Technological innovations to come. Beyond the exciting array of capabilities of emerging techniques, further developments are likely around the corner. For example, although multimodal measurements are possible, with increases in the multiplexing in all modalities, it could be possible to leverage spatially resolved genome-wide measurements at cellular resolution to derive single-cell phenotype atlases with spatial information from a single experiment. Similarly, metabolic profiling of small molecules, lipids and drugs has yet to be incorporated with emerging spatial profiling techniques, although imaging mass spectrometry offers this promise. Finally, the vast majority of tissues are 3D structures, and extending spatial profiling, be it via consecutive 2D sections¹⁸² or 3D imaging¹⁷⁷, offers the opportunity to build 3D atlases of cells¹⁸³ and tissues⁸¹. On all of these fronts, novel computational methods will be needed to integrate data across multiple modalities and length scales¹⁸⁴ to provide access to the insights provided by such comprehensive measurement of the molecular architecture of cells and tissues.

Data and clinical integration. As single or multimodal spatial profiling techniques become increasingly available, we envision that such methods will greatly inform clinical diagnostics and prognostics. However, first informative features must be learned through the integration of high-content screens (for example, ST profiling) with clinical metadata (for example, survival or response). Here, in addition to omics information, spatial context provides an additional layer to increase predictive power through cell- and tissue-scale features, such as cell–cell interaction or invasive cell behaviour, respectively. For example, in a single test, spatial transcriptome analysis could enable the identification of cancer gene signatures (for example, PAM50 for breast cancer), the proliferative and invasive potential of a tumour, as well as the degree of stromal and immune

cell infiltration for cancer subtyping and distinguishing immunogenic from cold tumours, respectively. Applied across large cohorts and including additional genetic modalities (for example, T cell receptor and B cell receptor sequencing for clonal amplification of tumour-reactive immune cells or the identification of tertiary lymphoid organs) and epigenetic markers (for example, spatial ATAC¹⁸⁵ or CUT&Tag for histone¹⁸⁶ profiling), it becomes an iterative learning process, in which increasing amounts of data gradually increase predictive feature numbers for improved prediction.

Reference atlases. A key requirement for the charting of diseased tissues will be the precise characterization of healthy tissues to distinguish healthy from diseased areas and normal from altered cells. In many ways, providing these healthy reference points is the ambitious goal of the Human Cell Atlas project, which aims to provide a catalogue of all healthy human cell types in terms of molecular composition, morphology and location¹⁸⁷, and is just one of many ambitious cell atlas projects. To date, such efforts have largely been powered by massive application of dissociated single-cell techniques (for example, scRNA-seq) on tissues and organs^{188–190}, with efforts to represent the global human ethnic diversity. As spatial profiling techniques mature and are more widely adopted, we fully expect that these approaches will play a pivotal part in such atlas-building efforts, as single-cell and spatial profiles synergize through the high-throughput molecular phenotyping capacity of the former and the conserved cell and tissue architecture profiling of the latter. Beyond spatial context, spatial profiling methods offer other advantages that derive from the lack of dissociation, including the ability to profile tightly connected (for example, neurons)

or dissociation-sensitive (for example, neutrophils) cell types, or from increased sensitivity, for example, the ability to profile lowly expressed but functionally relevant genes, such as those encoding receptors or transcription factors, and define subtle differences in cell type and cell state defined by these genes. Given the respective promise of these techniques, it is paramount to find ways to merge dissociated-cell and spatial profiling methods. Integrative genome-wide single-cell and spatial approaches range from the screening of gene markers and signatures to the spatial projection of cell types and states¹⁹¹. Furthermore, single-cell atlases are a resource for the design of targeted panels for image-based transcriptomics or spatial protein approaches to generate integrated spatially resolved atlases.

Conclusions

With spatial methods gaining robustness, scalability and access, we foresee their broader implementation in many areas of life science, from basic to clinical research. Eventually their application in areas such as pathology or drug development can further contribute to modernize and personalize health care. Until then, the diverse landscape of technologies and modalities will require coordinated efforts to benchmark and standardize processes to ensure reliable and reproducible results. Although such efforts have been undertaken for single-cell methods^{192,193}, their application to spatial and multi-omics methods will drive future informed decision-making processes. Together, spatial profiling is being established as a major player in the research and clinical communities and, no doubt, will further revolutionize our understanding of the complexity of life.

Published online 20 July 2022

- Elmentaita, R., Domínguez Conde, C., Yang, L. & Teichmann, S. A. Single-cell atlases: shared and tissue-specific cell types across human organs. *Nat. Rev. Genet.* **23**, 395–410 (2022).
- Fawkner-Corbett, D. et al. Spatiotemporal analysis of human intestinal development at single-cell resolution. *Cell* **184**, 810–826 (2021).
- Elmentaita, R. et al. Cells of the human intestinal tract mapped across space and time. *Nature* **597**, 250–255 (2021).
- Asp, M. et al. A spatiotemporal organ-wide gene expression and cell atlas of the developing human heart. *Cell* **179**, 1647–1660 (2019).
- Litvinuková, M. et al. Cells of the adult human heart. *Nature* **588**, 466–472 (2020).
- Asp, M. et al. Spatial detection of fetal marker genes expressed at low level in adult human heart tissue. *Sci. Rep.* **7**, 1–10 (2017).
- Kuppe, C. et al. Spatial multi-omic map of human myocardial infarction. Preprint at *bioRxiv* <https://doi.org/10.1101/2020.12.08.411686> (2020).
- Thrane, K., Eriksson, H., Maaskola, J., Hansson, J. & Lundeberg, J. Spatially resolved transcriptomics enables dissection of genetic heterogeneity in stage III cutaneous malignant melanoma. *Cancer Res.* **78**, 5970–5979 (2018).
- Ji, A. L. et al. Multimodal analysis of composition and spatial architecture in human squamous cell carcinoma. *Cell* **182**, 497–514 (2020).
- Moncada, R. et al. Integrating microarray-based spatial transcriptomics and single-cell RNA-seq reveals tissue architecture in pancreatic ductal adenocarcinomas. *Nat. Biotechnol.* **38**, 333–342 (2020).
- Nieto, P. et al. A single-cell tumor immune atlas for precision oncology. *Genome Res.* **31**, 1913–1926 (2021).
- Wu, Y. et al. Spatiotemporal immune landscape of colorectal cancer liver metastasis at single-cell level. *Cancer Discov.* **12**, 134–153 (2022).
- Pascual, G. et al. Dietary palmitic acid promotes a prometastatic memory via Schwann cells. *Nature* **599**, 485–490 (2021).
- Stähli, P. L. et al. Visualization and analysis of gene expression in tissue sections by spatial transcriptomics. *Science* **353**, 78–82 (2016). **The first publication to introduce the concept of spatial indexing with subsequent transcriptome readout using NGS.**
- Salmén, F. et al. Barcoded solid-phase RNA capture for spatial transcriptomics profiling in mammalian tissue sections. *Nat. Protoc.* **13**, 2501–2534 (2018).
- Kvastad, L. et al. The spatial RNA integrity number assay for *in situ* evaluation of transcriptome quality. *Commun. Biol.* **4**, 57 (2021).
- Lebrigand, K. et al. The spatial landscape of gene expression isoforms in tissue sections. Preprint at *bioRxiv* <https://doi.org/10.1101/2020.08.24.252296> (2022).
- Meylan, M. et al. Tertiary lymphoid structures generate and propagate anti-tumor antibody-producing plasma cells in renal cell cancer. *Immunity* **55**, 527–541 (2022).
- Villacampa, E. G. et al. Genome-wide spatial expression profiling in FFPE tissues. *Cell Genomics* **1**, 100065 (2021).
- Rodrigues, S. G. et al. Slide-seq: a scalable technology for measuring genome-wide expression at high spatial resolution. *Science* **363**, 1463–1467 (2019).
- Macosko, E. Z. et al. Highly parallel genome-wide expression profiling of individual cells using nanoliter droplets. *Cell* **161**, 1202–1214 (2015).
- Stickels, R. R. et al. Highly sensitive spatial transcriptomics at near-cellular resolution with slide-seqV2. *Nat. Biotechnol.* **39**, 313–319 (2021).
- Elosua-Bayes, M., Nieto, P., Mereu, E., Gut, I. & Heyn, H. SPOTlight: seeded NMF regression to deconvolute spatial transcriptomics spots with single-cell transcriptomes. *Nucleic Acids Res.* **49**, e50 (2021).
- Vickovic, S. et al. High-definition spatial transcriptomics for *in situ* tissue profiling. *Nat. Methods* **16**, 987–990 (2019). **This study presents the first spatial indexing methods with capture units at subcellular scale.**
- Chen, A. et al. Spatiotemporal transcriptomic atlas of mouse organogenesis using DNA nanoball-patterned arrays. *Cell* **185**, 1777–1792 (2022). **This paper reports high-resolution spatial indexing methods with nanometre-scale transcriptome capture units.**
- Drmanac, R. et al. Human genome sequencing using unchained base reads on self-assembling DNA nanoarrays. *Science* **327**, 78–81 (2010).
- Wang, M. et al. High-resolution 3D spatiotemporal transcriptomic maps of developing *Drosophila* embryos and larvae. *Dev. Cell* **57**, 1271–1283 (2022).
- Liu, C. et al. Spatiotemporal mapping of gene expression landscapes and developmental trajectories during zebrafish embryogenesis. *Dev. Cell* **57**, 1284–1298 (2022).
- Xia, K. et al. The single-cell stereo-seq reveals region-specific cell subtypes and transcriptome profiling in *Arabidopsis* leaves. *Dev. Cell* **57**, 1299–1310 (2022).
- Cho, C.-S. et al. Microscopic examination of spatial transcriptome using Seq-Scope. *Cell* **184**, 3559–3572 (2021).
- Bentley, D. R. et al. Accurate whole human genome sequencing using reversible terminator chemistry. *Nature* **456**, 53–59 (2008).

32. Fu, X. et al. Continuous polony gels for tissue mapping with high resolution and RNA capture efficiency. Preprint at *bioRxiv* <https://doi.org/10.1101/2021.03.17.435795> (2021).
33. Mitra, R. D. & Church, G. M. In situ localized amplification and contact replication of many individual DNA molecules. *Nucleic Acids Res.* **27**, e34 (1999).
34. Lee, Y. et al. XYZed: spatially resolved single-cell RNA sequencing reveals expression heterogeneity in the tumor microenvironment. *Sci. Adv.* **7**, eabg4755 (2021).
35. Srivatsan, S. R. et al. Embryo-scale, single-cell spatial transcriptomics. *Science* **373**, 111–117 (2021). **This publication describes a spatial method using combinatorial indexing to combine spatial indexing with subsequent single-cell sequencing.**
36. Srivatsan, S. R. et al. Massively multiplex chemical transcriptomics at single-cell resolution. *Science* **367**, 45–51 (2020).
37. Espina, V. et al. Laser-capture microdissection. *Nat. Protoc.* **1**, 586–603 (2006).
38. Qiu, S. et al. Single-neuron RNA-seq: technical feasibility and reproducibility. *Front. Genet.* **3**, 124 (2012).
39. Cadwell, C. R. et al. Electrophysiological, transcriptomic and morphologic profiling of single neurons using Patch-seq. *Nat. Biotechnol.* **34**, 199–203 (2016).
40. Subkhankulova, T., Yano, K., Robinson, H. P. C. & Livesey, F. J. Grouping and classifying electrophysiologically-defined classes of neocortical neurons by single cell, whole-genome expression profiling. *Front. Mol. Neurosci.* **3**, 10 (2010).
41. Lovatt, D. et al. Transcriptome in vivo analysis (TIVA) of spatially defined single cells in live tissue. *Nat. Methods* **11**, 190–196 (2014). **This paper introduces the concept of targeted labelling tissue regions of interest with subsequent next-generation transcriptome sequencing readout.**
42. Medaglia, C. et al. Spatial reconstruction of immune niches by combining photoactivatable reporters and scRNA-seq. *Science* **358**, 1622 (2021).
43. Hu, K. H. et al. ZipSeq: barcoding for real-time mapping of single cell transcriptomes. *Nat. Methods* **17**, 833–843 (2020).
44. Deiters, A. Light activation as a method of regulating and studying gene expression. *Curr. Opin. Chem. Biol.* **13**, 678–686 (2009).
45. Khan, M. et al. Visualizing in deceased COVID-19 patients how SARS-CoV-2 attacks the respiratory and olfactory mucosae but spares the olfactory bulb. *Cell* **184**, 5932–5949 (2021).
46. Liu, Y. et al. High-spatial-resolution multi-omics sequencing via deterministic barcoding in tissue. *Cell* **183**, 1665–1681 (2020).
47. Stoeckius, M. et al. Simultaneous epitope and transcriptome measurement in single cells. *Nat. Methods* **14**, 865–868 (2017).
48. Cao, J. et al. The single-cell transcriptional landscape of mammalian organogenesis. *Nature* **566**, 496–502 (2019).
49. Chen, K. H., Boettiger, A. N., Moffitt, J. R., Wang, S. & Zhuang, X. RNA imaging, spatially resolved, highly multiplexed RNA profiling in single cells. *Science* **348**, aaa6090 (2015). **This study introduces MERFISH and demonstrates that multiplexed FISH-based methods could multiplex hundreds to a thousand genes with high detection efficiency.**
50. Xia, C., Fan, J., Emanuel, G., Hao, J. & Zhuang, X. Spatial transcriptome profiling by MERFISH reveals subcellular RNA compartmentalization and cell cycle-dependent gene expression. *Proc. Natl. Acad. Sci. USA* **116**, 19490–19499 (2019). **Together with Eng et al., this paper shows that multiplexed FISH-based methods can be used to profile ~10,000 genes.**
51. Eng, C.-H. L. et al. Transcriptome-scale super-resolved imaging in tissues by RNA seqFISH. *Nature* **568**, 235–239 (2019). **Together with Xia et al., this paper shows that multiplexed FISH-based methods can be used to profile ~10,000 genes.**
52. Emanuel, G., Moffitt, J. R. & Zhuang, X. High-throughput, image-based screening of pooled genetic-variant libraries. *Nat. Methods* **14**, 1159–1162 (2017).
53. Wang, C., Lu, T., Emanuel, G., Babcock, H. P. & Zhuang, X. Imaging-based pooled CRISPR screening reveals regulators of lncRNA localization. *Proc. Natl. Acad. Sci. USA* **116**, 10842–10851 (2019).
54. Frieda, K. L. et al. Synthetic recording and in situ readout of lineage information in single cells. *Nature* **541**, 107–111 (2017).
55. Chow, K.-H. K. et al. Imaging cell lineage with a synthetic digital recording system. *Science* **372**, eabb3099 (2021).
56. Chen, X. et al. High-throughput mapping of long-range neuronal projection using in situ sequencing. *Cell* **179**, 772–786 (2019).
57. Sun, Y.-C. et al. Integrating barcoded neuroanatomy with spatial transcriptional profiling enables identification of gene correlates of projections. *Nat. Neurosci.* **24**, 873–885 (2021).
58. Feldman, D. et al. Optical pooled screens in human cells. *Cell* **179**, 787–799 (2019).
59. Zhuang, X. Spatially resolved single-cell genomics and transcriptomics by imaging. *Nat. Methods* **18**, 18–22 (2021).
60. Rao, A., Barkley, D., França, G. S. & Yanai, I. Exploring tissue architecture using spatial transcriptomics. *Nature* **596**, 211–220 (2021).
61. Close, J. L., Long, B. R. & Zeng, H. Spatially resolved transcriptomics in neuroscience. *Nat. Methods* **18**, 23–25 (2021).
62. Moses, L. & Pachter, L. Museum of spatial transcriptomics. *Nat. Methods* **19**, 534–546 (2022).
63. Ke, R. et al. In situ sequencing for RNA analysis in preserved tissue and cells. *Nat. Methods* **10**, 857–860 (2013). **This study introduces the use of padlock probes and rolling circle amplification for targeted in situ sequencing.**
64. Banér, J., Nilsson, M., Mendel-Hartvig, M. & Landegren, U. Signal amplification of padlock probes by rolling circle replication. *Nucleic Acids Res.* **26**, 5073–5078 (1998).
65. Larsson, C., Grundberg, I., Söderberg, O. & Nilsson, M. In situ detection and genotyping of individual mRNA molecules. *Nat. Methods* **7**, 395–397 (2010).
66. Daubendiek, S. L. & Kool, E. T. Generation of catalytic RNAs by rolling transcription of synthetic DNA nanocircles. *Nat. Biotechnol.* **15**, 273–277 (1997).
67. Zhang, D. Y., Brandwein, M., Hsu, T. C. & Li, H. Amplification of target-specific, ligation-dependent circular probe. *Gene* **211**, 277–285 (1998).
68. Tiklová, K. et al. Single-cell RNA sequencing reveals midbrain dopamine neuron diversity emerging during mouse brain development. *Nat. Commun.* **10**, 581 (2019).
69. Soldatov, R. et al. Spatiotemporal structure of cell fate decisions in murine neural crest. *Science* **364**, eaas9536 (2019).
70. Partel, G. et al. Automated identification of the mouse brain's spatial compartments from in situ sequencing data. *BMC Biol.* **18**, 144 (2020).
71. Qian, X. et al. Probabilistic cell typing enables fine mapping of closely related cell types in situ. *Nat. Methods* **17**, 101–106 (2020).
72. Chen, W.-T. et al. Spatial transcriptomics and in situ sequencing to study Alzheimer's disease. *Cell* **182**, 976–991 (2020).
73. Floridida, E. M. et al. Distinct oligodendrocyte populations have spatial preference and different responses to spinal cord injury. *Nat. Commun.* **11**, 5860 (2020).
74. Carow, B. et al. Spatial and temporal localization of immune transcripts defines hallmarks and diversity in the tuberculosis granuloma. *Nat. Commun.* **10**, 1823 (2019).
75. Svedlund, J. et al. Generation of in situ sequencing based OncoMaps to spatially resolve gene expression profiles of diagnostic and prognostic markers in breast cancer. *EBioMedicine* **48**, 212–223 (2019).
76. Lundin, E. et al. Spatiotemporal mapping of RNA editing in the developing mouse brain using in situ sequencing reveals regional and cell-type-specific regulation. *BMC Biol.* **18**, 6 (2020).
77. Zaghloul, A. et al. Expression profiling and in situ screening of circular RNAs in human tissues. *Sci. Rep.* **8**, 16953 (2018).
78. Liu, S. et al. Barcoded oligonucleotides ligated on RNA amplified for multiplexed and parallel in situ analyses. *Nucleic Acids Res.* **49**, e58 (2021).
79. Wang, X. et al. Three-dimensional intact-tissue sequencing of single-cell transcriptional states. *Science* **361**, aat5691 (2018). **This reference introduces starMAP and the use of SNAIL probes to generate RCPs without cDNA synthesis.**
80. He, Y. et al. ClusterMap for multi-scale clustering analysis of spatial gene expression. *Nat. Commun.* **12**, 5909 (2021).
81. Alon, S. et al. Expansion sequencing: spatially precise in situ transcriptomics in intact biological systems. *Science* **371**, eaax2656 (2021).

This study uses expansion microscopy to improve the efficiency and resolution of targeted and untargeted in situ sequencing with the technique ExSeq.

82. Chen, F., Tillberg, P. W. & Boyden, E. S. Optical imaging. Expansion microscopy. *Science* **347**, 543–548 (2015).
83. Chen, F. et al. Nanoscale imaging of RNA with expansion microscopy. *Nat. Methods* **13**, 679–684 (2016).
84. Mignardi, M. et al. Oligonucleotide gap-fill ligation for mutation detection and sequencing in situ. *Nucleic Acids Res.* **43**, e151 (2015).
85. Chen, X., Sun, Y.-C., Church, G. M., Lee, J. H. & Zador, A. M. Efficient in situ barcode sequencing using padlock probe-based BaristaSeq. *Nucleic Acids Res.* **46**, e22 (2018).
86. Lee, J. H. et al. Highly multiplexed subcellular RNA sequencing in situ. *Science* **343**, 1360–1363 (2014). **This reference introduces FISSEQ, an untargeted in situ sequencing method.**
87. Lee, J. H. et al. Fluorescent in situ sequencing (FISSEQ) of RNA for gene expression profiling in intact cells and tissues. *Nat. Protoc.* **10**, 442–458 (2015).
88. Femino, A. M., Fay, F. S., Fogarty, K. & Singer, R. H. Visualization of single RNA transcripts in situ. *Science* **280**, 585–590 (1998).
89. Raj, A., van den Boogaard, P., Rifkin, S. A., van Oudenaarden, A. & Tyagi, S. Imaging individual mRNA molecules using multiple singly labeled probes. *Nat. Methods* **5**, 877–879 (2008).
90. Battich, N., Stoeger, T. & Pelkmans, L. Image-based transcriptomics in thousands of single human cells at single-molecule resolution. *Nat. Methods* **10**, 1127–1133 (2013).
91. Levsky, J. M., Shenoy, S. M., Pezo, R. C. & Singer, R. H. Single-cell gene expression profiling. *Science* **297**, 836–840 (2002).
92. Lubeck, E. & Cai, L. Single-cell systems biology by super-resolution imaging and combinatorial labeling. *Nat. Methods* **9**, 743–748 (2012).
93. Jakt, L. M., Moriwaki, S. & Nishikawa, S. A continuum of transcriptional identities visualized by combinatorial fluorescent in situ hybridization. *Development* **140**, 216–225 (2013).
94. Levesque, M. J. & Raj, A. Single-chromosome transcriptional profiling reveals chromosomal gene expression regulation. *Nat. Methods* **10**, 246–248 (2013).
95. Lubeck, E., Coskun, A. F., Zhiyentayev, T., Ahmad, M. & Cai, L. Single-cell in situ RNA profiling by sequential hybridization. *Nat. Methods* **11**, 360–361 (2014). **This paper introduces the core concept behind seqFISH and demonstrates the profiling of 12 RNAs.**
96. Moffitt, J. R. et al. High-throughput single-cell gene-expression profiling with multiplexed error-robust fluorescence in situ hybridization. *Proc. Natl. Acad. Sci. USA* **113**, 11046–11051 (2016).
97. Moffitt, J. R. et al. High-performance multiplexed fluorescence in situ hybridization in culture and tissue with matrix imprinting and clearing. *Proc. Natl. Acad. Sci. USA* **113**, 14456–14461 (2016).
98. Shah, S., Lubeck, E., Zhou, W. & Cai, L. In situ transcription profiling of single cells reveals spatial organization of cells in the mouse hippocampus. *Neuron* **92**, 342–357 (2016).
99. Shah, S. et al. Dynamics and spatial genomics of the nascent transcriptome by intron seqFISH. *Cell* **174**, 363–376 (2018).
100. Gyllborg, D. et al. Hybridization-based in situ sequencing (HybISS) for spatially resolved transcriptomics in human and mouse brain tissue. *Nucleic Acids Res.* **48**, e112 (2020).
101. Beliveau, B. J. et al. Versatile design and synthesis platform for visualizing genomes with Oligopaint FISH probes. *Proc. Natl. Acad. Sci. USA* **109**, 21301–21306 (2012).
102. Moffitt, J. R. & Zhuang, X. RNA imaging with multiplexed error-robust fluorescence in situ hybridization (MERFISH). *Methods Enzymol.* **572**, 1–49 (2016).
103. Kosuri, S. & Church, G. M. Large-scale de novo DNA synthesis: technologies and applications. *Nat. Methods* **11**, 499–507 (2014).
104. Eng, C.-H. L., Shah, S., Thomassie, J. & Cai, L. Profiling the transcriptome with RNA SPOTS. *Nat. Methods* **14**, 1153–1155 (2017).
105. Wang, G., Moffitt, J. R. & Zhuang, X. Multiplexed imaging of high density libraries of RNAs with MERFISH and expansion microscopy. *Sci. Rep.* **8**, 4847 (2018).
106. Xia, C., Babcock, H. P., Moffitt, J. R. & Zhuang, X. Multiplexed detection of RNA using MERFISH and

- branched DNA amplification. *Sci. Rep.* **9**, 7721 (2019).
107. Foreman, R. & Wollman, R. Mammalian gene expression variability is explained by underlying cell state. *Mol. Syst. Biol.* **16**, e9146 (2020).
 108. Su, J.-H., Zheng, P., Kinrot, S. S., Bintu, B. & Zhuang, X. Genome-scale Imaging of the 3D organization and transcriptional activity of chromatin. *Cell* **182**, 1641–1659 (2020).
 109. Moffitt, J. R. et al. Molecular, spatial, and functional single-cell profiling of the hypothalamic preoptic region. *Science* **362**, aau5324 (2018). **This study illustrates the potential for image-based transcriptomic methods to profile large tissue areas and numbers of cells by profiling 1.1 million cells.**
 110. Zhang, M. et al. Spatially resolved cell atlas of the mouse primary motor cortex by MERFISH. *Nature* **598**, 137–143 (2021).
 111. Favuzzi, E. et al. GABA-receptive microglia selectively sculpt developing inhibitory circuits. *Cell* **184**, 5686 (2021).
 112. Chen, R. et al. Decoding molecular and cellular heterogeneity of mouse nucleus accumbens. *Nat. Neurosci.* **24**, 1757–1771 (2021).
 113. Hara, T. et al. Interactions between cancer cells and immune cells drive transitions to mesenchymal-like states in glioblastoma. *Cancer Cell* **39**, 779–792 (2021).
 114. Lu, Y. et al. Spatial transcriptome profiling by MERFISH reveals fetal liver hematopoietic stem cell niche architecture. *Cell Discov.* **7**, 47 (2021).
 115. Liu, M. et al. Multiplexed imaging of nucleome architectures in single cells of mammalian tissue. *Nat. Commun.* **11**, 2907 (2020).
 116. Petukhov, V. et al. Cell segmentation in imaging-based spatial transcriptomics. *Nat. Biotechnol.* **40**, 345–354 (2022).
 117. Takei, Y. et al. Integrated spatial genomics reveals global architecture of single nuclei. *Nature* **590**, 344–350 (2021).
 118. Zhou, W. et al. Single-cell analysis reveals regulatory gene expression dynamics leading to lineage commitment in early T cell development. *Cell Syst.* **9**, 321–337 (2019).
 119. Lignell, A., Kerosuo, L., Streicher, S. J., Cai, L. & Bronner, M. E. Identification of a neural crest stem cell niche by spatial genomic analysis. *Nat. Commun.* **8**, 1830 (2017).
 120. Zhu, Q., Shah, S., Dries, R., Cai, L. & Yuan, G.-C. Identification of spatially associated subpopulations by combining scRNASeq and sequential fluorescence *in situ* hybridization data. *Nat. Biotechnol.* **36**, 1183–1190 (2018).
 121. Takei, Y. et al. Single-cell nuclear architecture across cell types in the mouse brain. *Science* **374**, 586–594 (2021).
 122. Kim, D. W. et al. Multimodal analysis of cell types in a hypothalamic node controlling social behavior. *Cell* **179**, 713–728 (2019).
 123. Lohoff, T. et al. Integration of spatial and single-cell transcriptomic data elucidates mouse organogenesis. *Nat. Biotechnol.* **40**, 74–85 (2022).
 124. Dirks, R. M. & Pierce, N. A. From the cover: triggered amplification by hybridization chain reaction. *Proc. Natl. Acad. Sci. USA* **101**, 15275–15278 (2004).
 125. Kishi, J. Y. et al. SABER amplifies FISH: enhanced multiplexed imaging of RNA and DNA in cells and tissues. *Nat. Methods* **16**, 533–544 (2019).
 126. Rouhanifard, S. H. et al. ClampFISH detects individual nucleic acid molecules using click chemistry-based amplification. *Nat. Biotechnol.* **37**, 84–89 (2018).
 127. Goh, J. J. L. et al. Highly specific multiplexed RNA imaging in tissues with split-FISH. *Nat. Methods* **17**, 689–693 (2020).
 128. Sountoulidis, A. et al. SCRINSHOT enables spatial mapping of cell states in tissue sections with single-cell resolution. *PLoS Biol.* **18**, e3000675 (2020).
 129. Nagendran, M., Riordan, D. P., Harbury, P. B. & Desai, T. J. Automated cell-type classification in intact tissues by single-cell molecular profiling. *eLife* **7**, e30510 (2018).
 130. Langseth, C. M. et al. Comprehensive *in situ* mapping of human cortical transcriptomic cell types. *Commun. Biol.* **4**, 998 (2021).
 131. La Manno, G. et al. Molecular architecture of the developing mouse brain. *Nature* **596**, 92–96 (2021).
 132. Codeluppi, S. et al. Spatial organization of the somatosensory cortex revealed by osmFISH. *Nat. Methods* **15**, 932–935 (2018).
 133. Dar, D., Dar, N., Cai, L. & Newman, D. K. Spatial transcriptomics of planktonic and sessile bacterial populations at single-cell resolution. *Science* **373**, eabi4882 (2021).
 134. Wang, Y. et al. EASI-FISH for thick tissue defines lateral hypothalamus spatio-molecular organization. *Cell* **184**, 6361–6377 (2021).
 135. Shaffer, S. M. et al. Rare cell variability and drug-induced reprogramming as a mode of cancer drug resistance. *Nature* **546**, 431–435 (2017).
 136. Coskun, A. F. & Cai, L. Dense transcript profiling in single cells by image correlation decoding. *Nat. Methods* **13**, 657–660 (2016).
 137. Cleary, B. et al. Compressed sensing for highly efficient imaging transcriptomics. *Nat. Biotechnol.* **39**, 936–942 (2021).
 138. Liu, Y., Beyer, A. & Aebersold, R. On the dependency of cellular protein levels on mRNA abundance. *Cell* **165**, 535–550 (2016).
 139. Angelo, M. et al. Multiplexed ion beam imaging of human breast tumors. *Nat. Med.* **20**, 436–442 (2014). **This paper introduces MIBI.**
 140. Keren, L. et al. A structured tumor-immune microenvironment in triple negative breast cancer revealed by multiplexed ion beam imaging. *Cell* **174**, 1373–1387 (2018).
 141. Risom, T. et al. Transition to invasive breast cancer is associated with progressive changes in the structure and composition of tumor stroma. *Cell* **185**, 299–310 (2022).
 142. Lundberg, E. & Borner, G. H. H. Spatial proteomics: a powerful discovery tool for cell biology. *Nat. Rev. Mol. Cell Biol.* **20**, 285–302 (2019).
 143. Taylor, M. J., Lukowski, J. K. & Anderton, C. R. Spatially resolved mass spectrometry at the single cell: recent innovations in proteomics and metabolomics. *J. Am. Soc. Mass. Spectrom.* **32**, 872–894 (2021).
 144. Buchberger, A. R., DeLaney, K., Johnson, J. & Li, L. Mass spectrometry imaging: a review of emerging advancements and future insights. *Anal. Chem.* **90**, 240–265 (2018).
 145. Coons, A. H., Creech, H. J. & Jones, R. N. Immunological properties of an antibody containing a fluorescent group. *Proc. Soc. Exp. Biol. Med.* **47**, 200–202 (1941).
 146. Hickey, J. W. et al. Spatial mapping of protein composition and tissue organization: a primer for multiplexed antibody-based imaging. *Nat. Methods* **19**, 284–295 (2022).
 147. Tan, W. C. C. et al. Overview of multiplex immunohistochemistry/immunofluorescence techniques in the era of cancer immunotherapy. *Cancer Commun.* **40**, 135–153 (2020).
 148. Bodenmiller, B. Multiplexed epitope-based tissue imaging for discovery and healthcare applications. *Cell Syst.* **2**, 225–238 (2016).
 149. Taube, J. M. et al. The society for immunotherapy of cancer statement on best practices for multiplex immunohistochemistry (IHC) and immunofluorescence (IF) staining and validation. *J. Immunother. Cancer* **8**, e000155 (2020).
 150. Du, Z. et al. Qualifying antibodies for image-based immune profiling and multiplexed tissue imaging. *Nat. Protoc.* **14**, 2900–2930 (2019).
 151. Uhlen, M. et al. A proposal for validation of antibodies. *Nat. Methods* **13**, 823–827 (2016).
 152. Chung, K. et al. Structural and molecular interrogation of intact biological systems. *Nature* **497**, 332–337 (2013).
 153. Li, W., Germain, R. N. & Gerner, M. Y. Multiplex, quantitative cellular analysis in large tissue volumes with clearing-enhanced 3D microscopy (C_3D). *Proc. Natl. Acad. Sci. USA* **114**, E7321–E7330 (2017).
 154. Murray, E. et al. Simple, scalable proteomic imaging for high-dimensional profiling of intact systems. *Cell* **163**, 1500–1514 (2015).
 155. Ku, T. et al. Multiplexed and scalable super-resolution imaging of three-dimensional protein localization in size-adjustable tissues. *Nat. Biotechnol.* **34**, 973–981 (2016).
 156. Park, Y.-G. et al. Protection of tissue physicochemical properties using polyfunctional crosslinkers. *Nat. Biotechnol.* **37**, 73–83 (2019).
 157. Richardson, D. S. et al. Tissue clearing. *Nat. Rev. Methods Prim.* **1**, 84 (2021).
 158. Gerdes, M. J. et al. Highly multiplexed single-cell analysis of formalin-fixed, paraffin-embedded cancer tissue. *Proc. Natl. Acad. Sci. USA* **110**, 11982–11987 (2013).
 159. Lin, J.-R., Fallahi-Sichani, M. & Sorger, P. K. Highly multiplexed imaging of single cells using a high-throughput cyclic immunofluorescence method. *Nat. Commun.* **6**, 8390 (2015).
 160. Lin, J.-R. et al. Highly multiplexed immunofluorescence imaging of human tissues and tumors using t-CyCIF and conventional optical microscopes. *eLife* **7**, e31657 (2018).
 161. Radtke, A. J. et al. IBEX: a versatile multiplex optical imaging approach for deep phenotyping and spatial analysis of cells in complex tissues. *Proc. Natl. Acad. Sci. USA* **117**, 33455–33465 (2020).
 162. Gut, G., Herrmann, M. D. & Pelkmans, L. Multiplexed protein maps link subcellular organization to cellular states. *Science* **361**, eaar7042 (2018). **This reference presents a highly multiplexed use of indirect IF (41) to study subcellular organization, demonstrating that 40 proteins can be visualized in the same cells.**
 163. Wahle, P. et al. Multimodal spatiotemporal phenotyping of human organoid development. Preprint at *bioRxiv* <https://doi.org/10.1101/2022.03.16.484396> (2022).
 164. Schubert, W. et al. Analyzing proteome topology and function by automated multidimensional fluorescence microscopy. *Nat. Biotechnol.* **24**, 1270–1278 (2006).
 165. Wählby, C., Erlandsson, F., Bengtsson, E. & Zetterberg, A. Sequential immunofluorescence staining and image analysis for detection of large numbers of antigens in individual cell nuclei. *Cytometry* **47**, 32–41 (2002).
 166. Wang, Y. et al. Rapid sequential *in situ* multiplexing with DNA exchange imaging in neuronal cells and tissues. *Nano Lett.* **17**, 6131–6139 (2017).
 167. Goltsev, Y. et al. Deep profiling of mouse splenic architecture with CODEX multiplexed imaging. *Cell* **174**, 968–981 (2018).
 168. Schürch, C. M. et al. Coordinated cellular neighborhoods orchestrate antitumoral immunity at the colorectal cancer invasive front. *Cell* **183**, 838 (2020). **This reference demonstrates 56-plex protein CODEX imaging across cohorts of tissue samples in a tissue microarray format. This represents the more commonly used implementation of CODEX based on hybridization–dehybridization.**
 169. Saka, S. K. et al. Immuno-SABER enables highly multiplexed and amplified protein imaging in tissues. *Nat. Biotechnol.* **37**, 1080–1090 (2019). **This paper demonstrates how DNA concatemers can be used for signal amplification without enzymatic reactions.**
 170. Zubarev, R. A. The challenge of the proteome dynamic range and its implications for in-depth proteomics. *Proteomics* **13**, 723–726 (2013).
 171. Lin, R. et al. A hybridization-chain-reaction-based method for amplifying immunosignals. *Nat. Methods* **15**, 275–278 (2018).
 172. Wang, Y. et al. Multiplexed *in situ* protein imaging using DNA-barcoded antibodies with extended hybridization chain reactions. Preprint at *bioRxiv* <https://doi.org/10.1101/274456> (2020).
 173. Tsujikawa, T. et al. Quantitative multiplex immunohistochemistry reveals myeloid-inflamed tumor-immune complexity associated with poor prognosis. *Cell Rep.* **19**, 203–217 (2017).
 174. Stack, E. C., Wang, C., Roman, K. A. & Hoyt, C. C. Multiplexed immunohistochemistry, imaging, and quantitation: a review, with an assessment of Tyramide signal amplification, multispectral imaging and multiplex analysis. *Methods* **70**, 46–58 (2014).
 175. Keren, L. et al. MIBI-TOF: a multiplexed imaging platform relates cellular phenotypes and tissue structure. *Sci. Adv.* **5**, eaax5851 (2019).
 176. Giesen, C. et al. Highly multiplexed imaging of tumor tissues with subcellular resolution by mass cytometry. *Nat. Methods* **11**, 417–422 (2014). **This paper introduces multiplexed imaging by mass cytometry and demonstrates the quantitative advantage and higher dynamic range of mass tag over fluorescence-based approaches.**
 177. Rovira-Clavé, X. et al. Subcellular localization of biomolecules and drug distribution by high-definition ion beam imaging. *Nat. Commun.* **12**, 4628 (2021).
 178. Manz, T. et al. Viv: multiscale visualization of high-resolution multiplexed bioimaging data on the web. *Nat. Methods* **19**, 515–516 (2022).
 179. Schapiro, D. et al. MITI minimum information guidelines for highly multiplexed tissue images. *Nat. Methods* **19**, 262–267 (2022).
 180. Fu, Y. et al. Pan-cancer computational histopathology reveals mutations, tumor composition and prognosis. *Nat. Cancer* **1**, 800–810 (2020).
 181. Sun, R. et al. A radiomics approach to assess tumour-infiltrating CD8 cells and response to anti-PD-1 or anti-PD-L1 immunotherapy: an imaging biomarker, retrospective multicohort study. *Lancet Oncol.* **19**, 1180–1191 (2018).

182. Ortiz, C. et al. Molecular atlas of the adult mouse brain. *Sci. Adv.* **6**, eabb3446 (2020).
183. Payne, A. C. et al. In situ genome sequencing resolves DNA sequence and structure in intact biological samples. *Science* **371**, eaay3446 (2021).
184. Qin, Y. et al. A multi-scale map of cell structure fusing protein images and interactions. *Nature* **600**, 536–542 (2021).
185. Deng, Y. et al. Spatial-ATAC-seq: spatially resolved chromatin accessibility profiling of tissues at genome scale and cellular level. Preprint at *bioRxiv* <https://doi.org/10.1101/2021.06.06.447244> (2021).
186. Deng, Y. et al. Spatial-CUT&Tag: spatially resolved chromatin modification profiling at the cellular level. *Science* **375**, 681–686 (2022). **This paper introduces the concept of spatial epigenomic profiling using spatial indexing of histone modifications using microfluidics.**
187. Regev, A. et al. The Human Cell Atlas. *eLife* **6**, e27041 (2017).
188. Tabula Sapiens Consortium. The Tabula sapiens: a multiple-organ, single-cell transcriptomic atlas of humans. *Science* **376**, eabl4896 (2022).
189. Domínguez Conde, C. et al. Cross-tissue immune cell analysis reveals tissue-specific features in humans. *Science* **376**, eabl5197 (2022).
190. Eraslan, G. et al. Single-nucleus cross-tissue molecular reference maps toward understanding disease gene function. *Science* **374**, eabl4290 (2022).
191. Longo, S. K., Guo, M. G., Ji, A. L. & Khavari, P. A. Integrating single-cell and spatial transcriptomics to elucidate intercellular tissue dynamics. *Nat. Rev. Genet.* **22**, 627–644 (2021).
192. Mereu, E. et al. Benchmarking single-cell RNA-sequencing protocols for cell atlas projects. *Nat. Biotechnol.* **38**, 747–755 (2020).
193. Ziegenhain, C. et al. Comparative analysis of single-cell RNA sequencing methods. *Mol. Cell* **65**, 631–643 (2017).
194. Ramani, V., Shendure, J. & Duan, Z. Understanding spatial genome organization: methods and insights. *Genomics Proteom. Bioinforma.* **14**, 7–20 (2016).
195. Dekker, J. & Mirny, L. The 3D genome as moderator of chromosomal communication. *Cell* **164**, 1110–1121 (2016).
196. Denker, A. & de Laat, W. The second decade of 3C technologies: detailed insights into nuclear organization. *Genes Dev.* **30**, 1357–1382 (2016).
197. Wang, S. et al. Spatial organization of chromatin domains and compartments in single chromosomes. *Science* **353**, 598–602 (2016).
198. Nir, G. et al. Walking along chromosomes with super-resolution imaging, contact maps, and integrative modeling. *PLoS Genet.* **14**, e1007872 (2018).
199. Mateo, L. J. et al. Visualizing DNA folding and RNA in embryos at single-cell resolution. *Nature* **568**, 49–54 (2019).
200. Cardozo-Gizzi, A. M. et al. Microscopy-based chromosome conformation capture enables simultaneous visualization of genome organization and transcription in intact organisms. *Mol. Cell* **74**, 212–222 (2019).
201. Nguyen, H. Q. et al. 3D mapping and accelerated super-resolution imaging of the human genome using *in situ* sequencing. *Nat. Methods* **17**, 822–832 (2020).
202. BRAIN Initiative Cell Census Network. A multimodal cell census and atlas of the mammalian primary motor cortex. *Nature* **598**, 86–102 (2021).
203. Bintu, B. et al. Super-resolution chromatin tracing reveals domains and cooperative interactions in single cells. *Science* **362**, eaau1783 (2018).

Acknowledgements

The authors thank M. Elosúa-Bayes and F. Björklund for support with the figure design. J.R.M. acknowledges funding from the Pew Charitable Trusts, the Helmsley Charitable Trust and the NIH (R01 GM143277, R21 CA249728). E.L. acknowledges funding from the Knut and Alice Wallenberg Foundation (KAW 2021.0346, KAW 2021.0189, KAW 2018.0172), Erling Persson Foundation, the NIH (U01 DK120447) and EU Horizon 2020 (EPIC-XS grant 823839 and ESPACE grant 874710). H.H. received support for the project PID2020-115439GB-I00 funded by MCIN/AEI/ 10.13039/501100011033. This publication is also supported as part of a project (BCLLATLAS and ESPACE) that has received funding from the European Research Council (ERC) under the European Union's Horizon 2020 Research and Innovation Programme (grant agreement nos. 810287 and 874710).

Author contributions

The authors contributed equally to all aspects of the article.

Competing interests

J.R.M. is a co-founder of, consultant for and scientific advisory board member of Vizgen, Inc. E.L. is adviser for Pixelgen technologies and Moleculent. H.H. is co-founder of Omniscope and scientific advisory board member of MirXES.

Peer review information

Nature Reviews Genetics thanks Je H. Lee, Sinem K. Saka and the other, anonymous, reviewer(s) for their contribution to the peer review of this work.

Publisher's note

Springer Nature remains neutral with regard to jurisdictional claims in published maps and institutional affiliations.

© Springer Nature Limited 2022